ÇUKUROVA UNIVERSITY
INSTITUTE OF NATURAL AND APPLIED SCIENCES

MSc. THESIS

Halit DOĞRUSÖZ

FINITE ELEMENT ANALYSIS AND TOPOLOGY OPTIMIZATION OF SHOCK ABSORBER YOKE ALONG WITH VISUALIZATION OF RESULTS IN AUGMENTED REALITY

DEPARTMENT OF MECHANICAL ENGINEERING

ADANA-2022

ÇUKUROVA UNIVERSITY
INSTITUTE OF NATURAL AND APPLIED SCIENCES

FINITE ELEMENT ANALYSIS AND TOPOLOGY OPTIMIZATION OF SHOCK ABSORBER YOKE ALONG WITH VISUALIZATION OF RESULTS IN AUGMENTED REALITY

Halit DOĞRUSÖZ

MSc. THESIS

DEPARTMENT OF MECHANICAL ENGINEERING

We certify that the thesis titled above was reviewed and approved for the award of degree of the Master of Science by the board of jury on 29/07/2022

……..……	…….....	……
Asst. Prof. Dr. M. İlteriş SARIGEÇİLİ SUPERVISOR	Assoc. Prof. Dr. Erinç ULUDAMAR MEMBER	Asst. Prof. Dr. Durmuş Ali BİRCAN MEMBER

This MSc. Thesis is written at the Department of Institute of Natural and Applied Sciences of Çukurova University.
Registration Number:

Prof. Dr. Sadık DİNÇER
Director
Institute of Natural and Applied Sciences

ABSTRACT

MSc. THESIS

FINITE ELEMENT ANALYSIS AND TOPOLOGY OPTIMIZATION OF SHOCK ABSORBER YOKE ALONG WITH VISUALIZATION OF RESULTS IN AUGMENTED REALITY

Halit DOĞRUSÖZ

ÇUKUROVA UNIVERSITY
INSTITUTE OF NATURAL AND APPLIED SCIENCES
DEPARTMENT OF MECHANICAL ENGINEERING

Supervisor : Asst. Prof. Dr. Mehmet İlteriş SARIGEÇİLİ
Year: 2022, Pages: 94
Jury : Asst. Prof. Dr. Mehmet İlteriş SARIGEÇİLİ
: Assoc. Prof. Dr. Erinç ULUDAMAR
: Asst. Prof. Dr. Durmuş Ali BIRCAN

Topology optimization is an effective technique for creating optimal designs that are impossible to achieve using traditional optimization techniques. While this technique is widely used for the designs subjected to static loads, it can also be used for optimization of the designs subjected to compliant designs that have challenging and complicated dynamic characteristics. In this study, the topology optimization method has been applied to a shock absorber yoke which is one of the most crucial components of an automobile. The component has been analyzed considering the side loads from suspension spring, top mount and lower bushing, additionally the annealing effect of lower tube end and 2.0 mm misalignment of lower bushing in longitudinal (X) direction. Then, the results have been visualized using augmented reality on a platform (i.e. tablet or phone) that supports this application using augmented reality. Visualizing the results in augmented reality on the physical component provides a new approach to the development of designs.

Keywords: Shock absorber, yoke, topology optimization, finite element analysis, FEA, augmented reality

ÖZ

YÜKSEK LİSANS TEZİ

AMORTİSÖR ÇATALININ SONLU ELEMANLAR ANALİZİ VE TOPOLOJİ OPTİMİZASYONU İLE BİRLİKTE SONUÇLARIN ARTIRILMIŞ GERÇEKLİKTE GÖRSELLEŞTİRİLMESİ

Halit DOĞRUSÖZ

ÇUKUROVA ÜNİVERSİTESİ
FEN BİLİMLERİ ENSTİTÜSÜ
MAKİNE MÜHENDİSLİĞİ ANABİLİM DALI

Danışman : Dr. Öğr. Üyesi Mehmet İlteriş SARIGEÇİLİ
Yıl: 2022, Sayfa: 94
Jüri : Dr. Öğr. Üyesi. Mehmet İlteriş SARIGEÇİLİ
: Doç. Dr. Erinç ULUDAMAR
: Dr. Öğr. Üyesi. Durmuş Ali BIRCAN

Topoloji optimizasyonu, geleneksel optimizasyon teknikleri kullanılarak elde edilmesi imkansız olan optimum tasarımlar oluşturmak için etkili bir tekniktir. Bu yöntem, statik yüklere maruz kalan tasarımlar için yaygın olarak kullanılmakla birlikte zorlu ve karmaşık dinamik özelliklere sahip uyumlu tasarımlara tabi tasarımların optimizasyonu için de kullanılabilir. Bu çalışmada, bir otomobilin en önemli bileşenlerinden biri olan amortisör çatalına topoloji optimizasyon yöntemi uygulanmıştır. Bileşen, süspansiyon yayı, üst montaj ve alt burçtan gelen yan yükler, ek olarak alt boru ucunun tavlama etkisi ve alt burcun boyuna (X) yönünde 2.0 mm yanlış hizalanması dikkate alınarak analiz edilmiştir. Daha sonra sonuçlar artırılmış gerçeklik kullanılarak bu uygulamayı destekleyen bir platformda (telefon gibi) görselleştirilmiştir. Sonuçların fiziksel bileşen üzerinde arttırılmış gerçeklikle görüntülenmesi, tasarımların geliştirilmesine yeni bir yaklaşım sağlar.

Anahtar Kelimeler: Amortisör, amortisör çatalı, topoloji optimizasyonu, sonlu elemanlar analizi, FEA, artırılmış gerçeklik

EXPANDED ABSTRACT

While the new regulations outweigh the carbon emissions in automotive industry, the use of lighter and unconventional parts has become necessary. Therefore, engineers have started to investigate methods of geometry optimization and material reduction. The topology optimization (TO) is a geometry optimization method that uses mathematical and algorithmic models to optimize the usage of the amount of material within a defined space for the defined set of conditions, loads and constraints. TO improves design performance and efficiency by removing excess material from regions that do not need to support large loads in order to minimize weight or solve design difficulties such as lowering resonance or thermal stress. The main objective of this optimization method is to evaluate and obtain the most suitable geometry of a vehicle's structural component to achieve the goals of performance and cost.

In order to start the finite element analysis (FEA) and topology optimization, the first requirement is to have an initial design which fulfills the packaging requirements of the given vehicle. This means that the initial rough geometry is an indication of the limit which can't be exceeded, otherwise the geometrical requirements and most importantly the vehicle safety requirements will be compromised. When an initial shock absorber design (including the rod, pressure tube, suspension spring, top mount, piston, compression and rebound system) is agreed upon, a CAD model is created. The dimensioning of the shock absorber is achieved from the rigid points and kinematics which are stated by the customer. Additional requirements are the information such as the weight of the vehicle, the foreseen maximum compression and rebound forces etc.

After defining the initial CAD model, next step is to define the load and boundary conditions. For the shock absorbers, there are two main loads that needs to be considered when it comes to the durability of the product: compression loads

and side loads. Firstly, as the maximum load deflection is defined by the customer (can be modified due to the component restrictions), the shock absorber is subjected to tests in compressed shock position (i.e. compressed length - CL). Secondly, the side loads which are caused by the module components such as suspension spring, lower bushing and top mount are defined. Additional to these loads, the bolt pre-tension load which is in fact used for clamping the yoke in the test rig or inside the car is defined.

The optimization of the form of the yoke is carried on using FEA to determine where the material should be focused on and which areas can be set to void. The implementations of the optimizations do not take into account the manufacturing possibilities. The structures which are generated after the FEA are often very difficult to manufacture or impossible in conventional ways. There are several ways to manufacture the generated structure and one of them is 3D printing. Additive manufacturing is one of the manufacturing ways that overcomes the limits which are often set by conventional production methods. It helps to implement a very easy way to manufacture extremely complicated structures. But since this method will result in having greater costs and relatively slower production speed, it is not preferred to use for this part. Therefore, before the production steps and investments begin, many restorations and improvements are necessary. Another set of FEA are needed to be completed in order to be certain that the decided design which is suited for production will comply with the given constraints and loads.

FEA results are obviously first obtained in a computer environment. An engineer can easily investigate and export a report with the use of software such as ANSYS, Abacus etc. Augmented reality allows engineers to investigate the superimposition of their digital information on a real-world environment that provides an opportunity to combine simulation results onto a real-world object. This study shows the ability to view the results of FEA for a designed part on the physical part.

GENİŞLETİLMİŞ ÖZET

Yeni düzenlemeler, otomotiv endüstrisinde karbon emisyonları açısından ağır basarken, daha hafif ve alışılmışın dışında parçaların kullanımı zorunlu hale gelmiştir. Bu nedenle mühendisler, geometri optimizasyonu ve malzeme azaltma yöntemlerini araştırmaya başladılar. Topoloji optimizasyonu (TO), tanımlanmış koşullar, yükler ve kısıtlamalar için tanımlanmış bir alan içindeki malzeme miktarının kullanımını optimize etmek için matematiksel ve algoritmik modelleri kullanan bir geometri optimizasyon yöntemidir. TO, ağırlığı en aza indirmek ya da rezonans veya termal stresi azaltmak gibi tasarım zorluklarını çözmek için büyük yükleri desteklemesi gerekmeyen bölgelerden fazla malzemeyi kaldırarak tasarım performansını ve verimliliğini artırır. Bu optimizasyon yönteminin temel amacı, performans ve maliyet hedeflerine ulaşmak için araç yapısal bileşenlerinin en uygun geometrisini elde etmektir.

Topoloji optimizasyonu ve sonlu elemanlar analizini (FEA) başlatmak için ilk şart, verilen aracın paketleme gereksinimlerini karşılayan bir başlangıç tasarımına sahip olmaktır. Bu, başlangıçtaki kaba geometrinin aşılamayacak sınırın bir göstergesi olduğu anlamına gelir, aksi takdirde geometrik gereksinimler ve en önemlisi araç güvenlik gereksinimleri tehlikeye girer. Bir ilk amortisör tasarımı (rot, iç basınç borusu, süspansiyon yayı, üst montaj, piston, sıkıştırma ve geri tepme sistemi dahil) üzerinde anlaşmaya varıldığında, bir CAD modeli oluşturulur. Amortisörün boyutlandırılması, müşteri tarafından belirtilen rijit noktalar ve kinematik ile sağlanır. Ek gereksinimler, aracın ağırlığı, öngörülen maksimum sıkıştırma ve geri tepme kuvvetleri vb. bilgilerdir.

Başlangıç CAD modelini tanımladıktan sonraki ilk adım, yük ve sınır koşullarını tanımlamaktır. Amortisörler için ürünün dayanıklılığı söz konusu olduğunda dikkate alınması gereken iki ana yük vardır: sıkıştırma yükleri ve yan yükler. İlk olarak, maksimum yük sapması müşteri tarafından tanımlandığı için

(bileşen kısıtlamaları nedeniyle değiştirilebilir), amortisör sıkıştırılmış şok pozisyonunda (CL) testlere tabi tutulur. İkinci olarak, süspansiyon yayı, alt burç ve üst montaj gibi modül bileşenlerinin neden olduğu yan yükler tanımlanır. Bu yüklere ek olarak, aslında çatalı test teçhizatında veya kabin içinde kenetlemek için kullanılan civata ön gerilim yükü tanımlanır.

Çatal formunun optimizasyonu, malzemenin nereye odaklanması gerektiğini ve hangi alanların boş olarak ayarlanabileceğini belirlemek için sonlu elemanlar analizi kullanılarak sürdürülür. Optimizasyon uygulamaları, imalat olanaklarını dikkate almaz. FEA analizinden sonra üretilen yapıların geleneksel yöntemlerle üretilmesi genellikle çok zordur veya imkansızdır. Oluşturulan yapıyı üretmenin birkaç yolu vardır ve bunlardan biri 3B baskıdır. Eklemeli üretim, genellikle geleneksel üretim yöntemlerinin koyduğu sınırları aşan üretim yollarından biridir. Son derece karmaşık yapıları üretmenin çok kolay bir yolunu uygulamaya yardımcı olur. Ancak bu yöntem daha yüksek maliyetlere ve nispeten daha yavaş üretim hızına neden olacağından bu kısım için kullanılması tercih edilmemektedir. Bu nedenle üretim aşamaları ve yatırımlar başlamadan önce birçok restorasyon ve iyileştirme yapılması gerekmektedir. Üretime uygun karar verilen tasarımın verilen kısıtlamalar ve yüklere uygun olacağından emin olmak için başka bir FEA analizi setinin tamamlanması gerekmektedir.

FEA analiz sonuçları açıkça ilk olarak bilgisayar ortamında elde edilmektedir. Bir mühendis, ANSYS, Abacus vb. gibi yazılımların kullanımıyla bir raporu kolayca araştırabilir ve dışa aktarabilir. Artırılmış gerçeklik, mühendislerin simülasyon sonuçlarını gerçek dünya nesnesi üzerinde birleştirme fırsatı sağlayan gerçek dünya ortamında dijital bilgilerinin üst üste bindirilmesini araştırmalarına olanak tanır. Bu çalışma, tasarlanmış bir parçanın FEA analizini fiziksel parça üzerinde görüntüleme yeteneğini göstermektedir.

.

ACKNOWLEDGEMENTS

I would like to thank my supervisor at Cukurova University Asst. Prof. Dr. Mehmet İlteriş SARIGEÇİLİ and Engineering Supervisor of Tenneco Inc. Poland Mr. Grzegorz Tomczuk. I am grateful and indebted to them for their assistance, valuable guidance, and encouragement extended to me.

I also must express my gratitude to my parents who have always supported and been with me while completing my degrees.

TABLE OF CONTENTS **PAGE**

ABSTRACT I
ÖZ…… II
EXPANDED ABSTRACT III
GENİŞLETİLMİŞ ÖZET V
ACKNOWLEDGEMENTS VII
TABLE OF CONTENTS VIII
LIST OF TABLES X
LIST OF FIGURES XII
LIST OF ABBREVIATIONS XVI
1. INTRODUCTION 1
1.1. Shock Absorbers 1
1.2. Topology Optimization Method 5
1.3. Augmented Reality 9
1.4. Motivation of the Study 9
2. PRELIMINARY WORK 11
2.1. Structural Topology Optimization 11
2.2. Structural Topology Optimization Applications in Automotive Industry 16
2.3. FEA-AR Integration 23
3. MATERIAL AND METHOD 27
3.1. Shock Absorber Design and Yoke Optimization 28
3.2. Design and Topology Optimization of the Yoke 36
3.3. Design Iteration - I 39
3.4. Design Iteration – II 43
3.5. Design Iteration – III 46
3.6. Augmented Reality Implementation 48
4. RESULTS AND DISCUSSION 61

4.1. Topology Optimization and Analysis Results 61
4.2. Augmented Reality Results..... 74
5. CONCLUSION..... 77
REFERENCES 81
CURRICULUM VITAE..... 87
APPENDIX 88
A.1. 38MnVS6 and EN 10083-2 Material Specifications 90
A.2. E235+C and E335+C Material Specifications..... 92

LIST OF TABLES **PAGE**

Table 2.1. Load cases specified for the jet engine bracket analysis 15
Table 2.2. Loading configurations..... 19
Table 3.1. Design requirements of a shock absorber..... 32
Table 3.2. Topology optimization analysis finite elements..... 39
Table 3.3. Static strength verification analysis finite elements. 39
Table 3.4. Material properties of the components. 42
Table 3.5. New material properties used in analysis 46
Table 3.6. Stiffness of lower bushing and top mount. 48
Table 4.1. Stress-strain and deflection results for F_1 and F_2 load cases. 62

LIST OF FIGURES **PAGE**

Figure 1.1. (A) Single-tube shock absorber and (B) Twin-tube shock absorber. 2
Figure 1.2. Triple tube shock absorber cross section view 4
Figure 1.3. Images representing FEA results of A) lower mesh quality B) higher mesh quality. 6
Figure 1.4. Discretization of a beam using SIMP method. Iterations completed A) 7%, B) 25%, C) 50%, D) 75%, E) 100%..... 7
Figure 2.1. One of the earliest solutions proposed for the structural topology optimization problem 12
Figure 2.2. (A) Office building in Japan, (B) Support structure optimized using TO and (C) A building in Doha using a support structure which is optimized using TO 13
Figure 2.3. (A) The design domain sandwiched between black material to mimic the resultant structure when stacking and bonding of the lattices, (B) optimized lattice structure, (C) the optimized lattice structure that is sliced to reveal the fluid streamlines..... 14
Figure 2.4. (A) A long slander beam which is subjected to F variable force (later in the research, this force is given as 10N, 15 N, 20 N and 30 N, optimal designs from (B) linear analysis, (C) materially non-linear analysis, (D) geometrically nonlinear analysis, (E) materially and geometrically nonlinear analysis 14
Figure 2.5. First iteration of TO..... 15
Figure 2.6. (A) Second iteration and (B) overlay of both iterations. 16
Figure 2.7. (A)Results of topology optimization of suspension by Kilian et al. (2003), (B) Results of topology optimization of a bracket..... 17

Figure 2.8. (A) Topology optimization results, (B) Size optimization with hypothetically manufacturable model (Cavazzuti et al., 2011). 18
Figure 2.9. (A) design space indicator, domain, (B) optimum configuration of the chassis, (C) optimum configuration of the roof 20
Figure 2.10. Forces (A) during steering, (B) during breaking, (C) when the suspension reaches its maximum stroke. 21
Figure 2.11. Final geometrical configuration of the rear suspension subframe analyzed for (A) during steering, (B) during breaking, (C) when the suspension reaches its maximum stroke 22
Figure 2.12. Product real-time view and AR visualization 23
Figure 2.13. Hyundai's AR application demonstration 24
Figure 2.14. Ferrari's Showroom app 25
Figure 3.1. (A) Damping force – path diagram (B) damping force – speed diagram. 28
Figure 3.2. McPherson and double-wishbone type suspension elements 31
Figure 3.3. 3D model of a vehicle's suspension components that designers rarely receive from requestors. 31
Figure 3.4. Module (also known as "strut") vs Shock absorber. 33
Figure 3.5. Shock absorber quarter-car modelling. 34
Figure 3.6. Module mountng angle and distance from lower wishbone pivot point. 35
Figure 3.7. Available design space for shock absorber yoke. 38
Figure 3.8. Topology analysis of the available packaging space with (A) 60% and (B) 70% volume reduction. 40
Figure 3.9. First concept design created by considering the output of the first topology optimization, based on packaging requirements and previous experience. 41
Figure 3.10. Second iteration topology optimization of the yoke and possible material reduction points. 44

Figure 3.11. Second iteration of the yoke design. 45
Figure 3.12. Cross section comparison of (A) second iteration and (B) first iteration yoke design. 45
Figure 3.13. Load case with a misalignment of 2mm from the center of sleeve. 47
Figure 3.14. Yoke designed for (A) Chinese load cases and (B) European load cases. 48
Figure 3.15. AR workflow and visualization of data. 49
Figure 3.16. Importing Vuforia Engine in Unity using Package Manager. 51
Figure 3.17. Model Target Generator interface. 52
Figure 3.18. Importing the 3D object which is obtained after FEA results. 53
Figure 3.19. Model orientation selection prior to import of the object. 53
Figure 3.20. Model Type options provided in the Model Target Generator software 54
Figure 3.21. Motion hint options provided in Model Target Generator software 55
Figure 3.22. Recognition range selection within Model Target Generator software. 56
Figure 3.23. Importing Vuforia Engine assets to the Unity environment. 57
Figure 3.24. 3D data view after import as model target. 57
Figure 3.25. Model Target setup panel. 58
Figure 3.26. Generated 2D guide view. 59
Figure 3.27. Build settings of Android and platform availability. 60
Figure 4.1. Summary of topology optimization results of three design iterations. 61
Figure 4.2. Von Mises, maximum and minimum principal stress [MPa] and equivalent plastic strain [-] distribution over (A) yoke and (B) tube under F_2 = 84kN (Tenneco CAE analysis report #2952). 63

Figure 4.3. Yoke - Von Mises, maximum and minimum principal stress [MPa] and equivalent plastic strain [-] distribution over (A) yoke and (B) tube under F_2 = -91kN (Tenneco CAE analysis report #3048). 65
Figure 4.4. Visible buckling of the second design iteration prototype shock absorber. 66
Figure 4.5. Load deflection graph for shock absorber which is equipped with two variants of yoke designs, 4 sets of load cases and misallignment. 66
Figure 4.6. Analysis results for (A) yoke variant 1 with (B) E235+C tube. Misalignment with maximum EU load case (Tenneco CAE analysis report #3455). 68
Figure 4.7. Analysis results for (A) yoke variant 1 with (B) E235+C tube. Misalignment with maximum Chinese load case that the shock absorber can handle (Tenneco CAE analysis report #3455). 70
Figure 4.8. Analysis results for (A) yoke variant 1 with (B) E335+C tube. Misalignment with maximum CH load case 91kN (Tenneco CAE analysis report #3455). 71
Figure 4.9. Analysis results for (A) Yoke variant 2 with (B) E335+C tube. Misalignment with maximum CH load case 91kN (Tenneco CAE analysis report #3455). 73
Figure 4.10. Exported 3D model of the yoke analysis results in the colors obtained after static analysis in Ansys. 74
Figure 4.11. Mobile view of (A) original 3D view of object, (B) object matched with the guide view, (C) rotated view of the object. 75
Figure 5.1. Complete assembly of shock absorber. 78

LIST OF ABBREVIATIONS

Δp	: Pressure difference [MPa]
2D	: 2 dimensional
3D	: 3 dimensional
AG	: Augmented reality
A_K	: Annular surface of double tube shock absorber [mm^2]
A_{KR}	: Annular surface single tube shock absorber [mm^2]
CAD	: Computer aided design
CL	: Compressed length
CNC	: Computer numerical control
d	: Rod diameter [mm]
D	: Oil chamber diameter [mm]
DL	: Design length
EL	: Extended length
FDM	: Fused deposition modelling
FEA	: Finite element analysis
FEM	: Finite element method
HMD	: Head-mounted display
LCA	: Lower control arm
$p(u)$	: Material density
$\dot{Q}_1$	: Volume flow between chambers of single tube shock absorber [mm^3/s]
$\dot{Q}_2$	: Volume flow between chambers of double tube shock absorber [mm^3/s]
SIMP	: Solid isotropic material with penalization
SLA	: Stereolithography
SLM	: Selective laser melting

SLS	: Selective laser sintering
TO	: Topology optimization
u	: Linearity and nonlinearity representant
$u(p)$	: Design space
VR	: Virtual reality
$\dot{z}$	: Speed of inward or outward movement of shock absorber [mm/s]
A_{tube}	: Selection of the pressure tube (m^2)
A_{rod}	: Section of the rod (m^2)
p_{gas}	: Gas pressure (Pa)
$F_{friction}$	: Force generated by friction (N)
F_{gas}	: Gas force (N)
F_{damper}	: Force generated by damper (N)
$F_{damping}$	: Damping force (N)
m	: Sprung mass (kg)
c	: Damping coefficient (Ns/m)
k	: Spring rate (N/m)

1. INTRODUCTION

1.1. Shock Absorbers

A shock absorber, or damper, reduces the effect of unwanted oscillations in order to increase the handling and comfort in a vehicle subjected to various dynamic forces some of which can be non-anticipated. Additionally, this component needs to comply with various operating conditions including loaded/unloaded, accelerating/braking, level/uneven road and straight/curved road. The damping force occurs while the shock absorber's fluid is forced through orifices at high velocities. Nowadays, hydraulic telescopic shock absorbers are used exclusively in motor vehicles as body shock absorbers; these convert the kinetic energy of the body and wheel vibrations into heat energy.

The damping effect of hydraulic telescopic shock absorbers is provided by the motion subjected to flow resistance of the piston equipped with damper valve which contains orifice and discs within oil filled chamber, also known as pressure tube. This energy conversion ends with the generated heat being released into the environment. Therefore, the difference of the pressure, Δp between the pressure tube and the surfaces of the moving elements on both sides of the damper generates the damping force $F_{damping}$ when the piston rod moves in and out.

The hydraulic telescopic shock absorbers can be investigated in three categories: single-tube, twin tube and triple-tube shock absorbers. The principle of the single-tube shock absorber (Figure 1.1.A) is to use the enclosed gas volume which is separated by the floating piston when balancing out the compression and extending piston rod volume. The gas volume is compressed according to the volume of the rod which enters in the event of compression of the shock absorber. Twin-tube shock absorbers (Figure 1.1.B) have an additional oil chamber which works as a compensator. Therefore, there is no floating piston that separates the oil and gas. The valves at the bottom of the pressure tube contains a valve that helps oil flow through the reserve tube in order to compensate the piston-rod volume.

The reserve tube is partially filled with oil and partially with gas. Generally, the gas pressure is atmospheric or slightly higher.

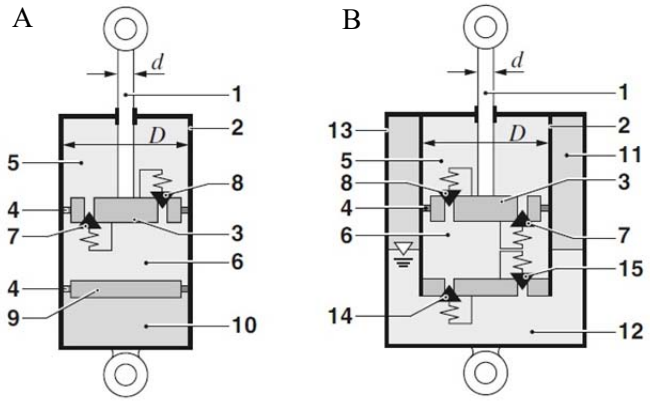


Figure 1.1. (A) Single-tube shock absorber and (B) Twin-tube shock absorber. (Dietsche et al., 2022).

The components numbered in Figure 1.1 are listed as follows:

1. Piston rod,
2. Working cylinder,
3. Piston,
4. Seal,
5. Oil chamber,
6. Secondary working chamber,
7. First valving,
8. Second valving,
9. Floating piston,
10. Gas,
11. Reserve tube gas filled area,
12. Reserve tube oil chamber,
13. Outer tube,

14. Reserve tube valve,
15. Second reserve tube valve.

A triple-tube shock absorber (Figure 1.2) is constituted mainly by a pressure tube, a reserve tube and a tube which is disposed between the pressure tube (generally called third-tube) and the intermediate tube. An O-ring is disposed between the pressure tube and the intermediate tube to provide sealing function between intermediate chamber and reserve chamber. The intermediate tube ends at a position spaced from a base valve to allow for the reduction of diameter of the reserve tube without adversely affecting the fluid flow (Nowaczyk and Paesmans, 2010).

The area which the pressure is prevailed on corresponds to an annular surface A_{KR} for the chamber through which the piston rod of the shock absorber is moving. The inner diameter of the pressure tube corresponds to diameter D and the piston outer diameter corresponds to diameter d. Then, the annular surface A_{KR} is defined as (Dietsche and Reif, 2022):

$$A_{KR} = \frac{\pi}{4}(D^2 - d^2) \tag{1.1}$$

For the double tube shock absorbers, the surface area equation contains only the pressure tube inner diameter because the volume of the piston rod is compensated by the reserve tube as follows:

$$A_K = \frac{\pi}{4}D^2 \tag{1.2}$$

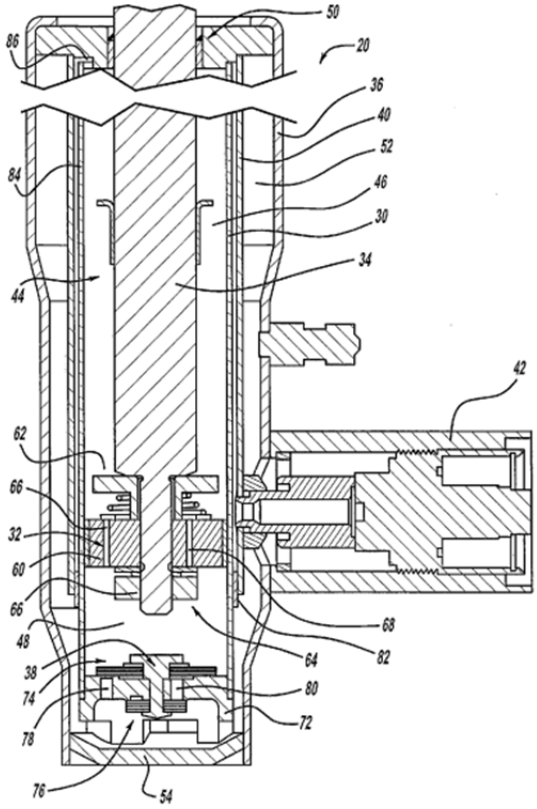


Figure 1.2. Triple tube shock absorber cross section view (Nowaczyk and Paesmans, 2010).

The volume of oil flows through the related valves depending on the type of the shock absorber and the speed of inward or outward movement, ż. The flow equation, Eq. (1.3), applies to the volume flow rate, $\dot{Q}_1$, between the two working chambers. The incompressibility of the shock absorber oil means that a possibility to compensate for the oil volume displaced or released by the piston rod is required. Eq. (1.4) applies to the volume flow rate $\dot{Q}_2$ (Dietsche and Reif, 2022):

$$\dot{Q}_1 = \frac{\pi}{4}(D^2 - d^2)\dot{z} \tag{1.3}$$

$$\dot{Q}_2 = \frac{\pi}{4} d^2 \dot{z} \quad (1.4)$$

Flow through characteristics are adjusted according to the characteristic of the vehicle and the type of the shock absorber that is selected for the vehicle (Dietsche and Reif, 2022).

1.2. Topology Optimization Method

In recent years, design engineers in automotive industry are facing challenges such as weight and material reduction for automobile components. The complexity of the parts increases due to changing loading conditions and constraints. This means that the design of a part needs to have less material but must stand the static and dynamic forces applied on it.

Setting up a minimum compliance design is a common optimization problem. The design seeks to optimize a simple mechanical structure to have the higher structural rigidity or lower compliance. Obviously, the mechanical structure will provide more stiffness when they are solid and have no voids. However, it might be desirable to reduce the weight of the structure for variety of reasons: saving the cost of material, saving fuel (e.g. in automotive and other vehicle industries) and to change the dynamic behavior.

In a topology optimization (TO) problem, boundary conditions should be defined first. It is desired to obtain a structure as stiff as possible in the given conditions and given weight reduction requirements. In most of the cases, when designing a shock absorber, due to the safety requirements, there are no weight reduction conditions. The structure must maintain its integrity and stiffness with as minimum weight as possible. Therefore, the optimization is carried out considering the fatigue limits of the part.

One of the most important tasks in carrying out a TO to discretize is to refine the mesh of the design, to determine whether the element is a void or solid

region. Mesh refinement is a process that can be defined as considering an existing mesh of a finite element model and changing the size, shape and/or order of the elements that creates the mesh to increase the accuracy of the solution as presented in Figure 1.3 (Staten et al., 1997). Many research has been concluded on refining the mesh. Some of the research has focused on two and three dimensional tetrahedral meshes (Rivara, 1991; Ning et al., 1993; Schneiders, 1995). It is obvious that every model which will be subjected to structural analysis needs to be discretized into smaller elements. However, this will result in a tradeoff between having more accurate results and increased computational times. When the generated mesh is too rough, it does not represent sufficiently the reality but on the other hand, the computation time required for the analysis will be shorter.

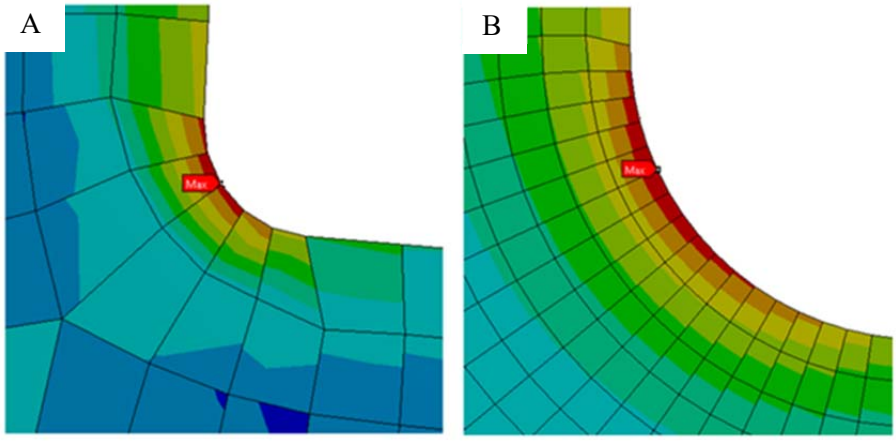


Figure 1.3. Images representing FEA results of (A) lower mesh quality (B) higher mesh quality.

One of the most commonly used type of structural optimization method is Solid Isotropic Material with Penalization (SIMP) (Bendsoe and Kikuchi, 1988; Rozvany and Zhou, 1992). This method helps to obtain the most suited material distribution within the defined design space and boundary conditions (Figure 1.4). The classic approach to topology optimization is to discretize a domain into a grid of finite elements known as isotropic solid microstructures. Each element is either

filled with material (represented with number 1) for locations that require material or emptied of material (represented with number 0) for regions where material can be removed.

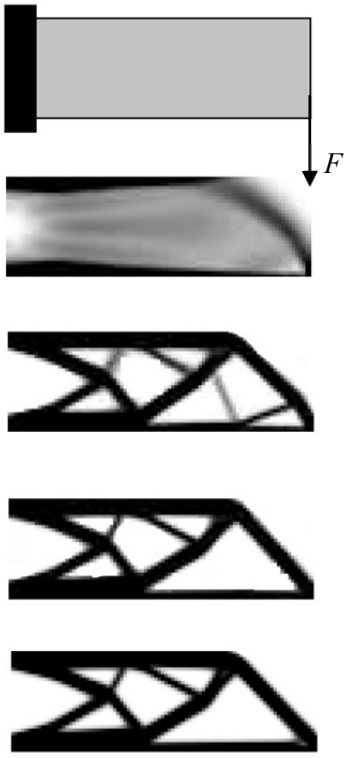


Figure 1.4. Discretization of a beam using SIMP method. Iterations completed A) 7%, B) 25%, C) 50%, D) 75%, E) 100% (Broxterman, 2017).

Topology optimization has attracted attention in many areas of engineering after its first publication by Bendsoe and Kikuchi (1988). Today, topology optimization is a method which is growing to be a very reliable and a must-have tool to improve the quality and the efficiency of the designs. One of the most challenging areas of manufacturing is the automotive industry as many conventional and unconventional manufacturing methods are used (Sehmi et al., 2018).

Automotive manufacturers and suppliers have begun to successfully implement the topology optimization methods in their designs over the years. One of the main usages of the topology optimization in automotive industry is the vehicle body/structure geometry optimization. Then, it is extended to the design of the weld patterns and optimal bead pattern design for the sheet metal parts of a vehicle (Yang et al., 1996). Also, this approach has been applied during the design of lower control arm (LCA), chassis brackets and fuel tanks (Yang et al., 2000) and many more automotive parts have been subjected to topology optimization methods.

The complexity of the problem is increasing as the number of variables change. Therefore, the problems with only ten variables can make it difficult to be solved. This is particularly the case when the optimization is carried out with gradient based algorithm and obtaining the gradient has to be done by evaluating the finite differences as it is often seen in solving practical engineering problems. When it comes to topology optimization, it is slightly different since the gradient information is available from the FEA results.

In automotive industry, additive manufacturing is being increasingly used for the purpose of both industry and research, mainly due to the generated complex design and results of the topology optimization. The use of additive manufacturing technologies such as 3D printing e.g., Fused Deposition Modelling (FDM), Stereolithography (SLA), Selective Laser Melting (SLM) and Selective Laser Sintering (SLS) has become widely used (Chuang et al., 2017). Conventional manufacturing methods such as CNC machining could fail to produce the obtained design due to the complexity of the design obtained after the optimization processes. As 3D printing devices/machines have become widely available, producing of unique designs which would require long and painful processing with conventional manufacturing methods became easier even though the after-analysis design requires modifications in order to be produced using 3D printing methods (Murr et al., 2012).

1.3. Augmented Reality

Augmented reality (AR) is a field of technology that helps to overlay a computer-generated object onto a real-world object in a way that the virtual object is aligned with the real-world objects. (Azuma, 1997). Development of the AR technologies has made it available for use in many fields such as education (Fonseca et al., 2014; Ibanez et al., 2014), engineering and research (Henderson et al., 2009; Irizarry et al., 2013) and entertainment industry (Haugstvedt et al., 2012).

The usage of AR in the industry can be seen in different categories as product development and maintenance, assembly tasks, architecture and planning (Dey et al., 2018). AR contributes to the improvement of the manufacturing and inspection on the factory floor. It also can assist designers in matching their designs on the physical objects. Additionally, it helps technicians to receive and read the technical documentation using their AR equipment without getting distracted[1].

1.4. Motivation of the Study

Topology optimization is a computer-based method which provides engineers with a wide range of possibilities and a bigger degree of freedom regarding the use of the available design space. Therefore, the desired mechanical performance is achieved much more effectively in terms of time and cost. Additionally, TO can help design engineers to think outside of the box during the design stage. As a result, many industries started to adapt the use of topology optimization in their design processes. With the improvement of digital FEA and new manufacturing technologies, topology optimization applications have seen rapid increase in the recent years. Especially in automotive industry where idea to real object time frame is very crucial, engineers prefer to use shorter ways to achieve their design targets. Therefore, the use of topology optimization has been

[1] https://www.softeq.com/blog/automotive-ar-innovative-application-areas-driving-the-industry#:~:text=Augmented%20reality%20applications%20used%20in,performance%2C%20weight%2C%20and%20financing (accessed by June, 2022)

promoted in this study. The final objects which are compliant to the defined loading conditions have been obtained after several iterations and each iteration was subjected to verification by performing FEA calculations.

It is possible to see if the topology optimization iss successful based on the FEA result. Also, visualizing the component on the prototype gives better insight to engineers on how to better optimize the design. There are numerous examples where augmented reality can be shown as a positive impact. For example, AR can be used to visualize an end product and provide assembly instructions of this component with user having to use only their smartphones or tablets[2]. Applications of AR have been previously used in visualizing the suspension out of a catalogue where the user was able to see a 3D model of the product[3]. However, visualizing analysis results on a physical shock absorber component using augmented reality have not been previously done. Therefore, in this study, FEA results of optimized design have been united.

[2] https://www.rs-online.com/designspark/augmented-reality-in-engineering (accessed by June, 2022)
[3] https://www.mupo.it/augmented-suspensions/?lang=en (accessed by June, 2022)

2. PRELIMINARY WORK

Finite element analysis is a first step for optimization of product design. It plays a very crucial role in the world of mechanical design and CAD engineering. The usage of it is most frequently done in mechanical engineering as well as civil engineering (Huang et al., 2016). An optimization of a mechanical component generally starts with performing analysis based on various fields of engineering such as structural analysis, flow and heat transfer analysis. In recent years, structural optimization became a fast-growing research field and many research has been done with the aim of finding the best suited structure for the given conditions and using as less material as possible.

As the technologies like virtual reality (VR) and augmented reality (AR) are implemented more in our lives, it is possible to see the usage of them in many fields and research has been concluded on them. Li et al. (2017; 2018) has carried out researches on AR technology being used in engineering analysis and presented their investigation on FEA-AR integration. First an overview on usage of AR for the engineering analysis and simulation were provided (Li et al., 2017) and then a prototype was implemented to demonstrate structural analysis of an object outdoors (Li et al., 2018). That system development of FEA result visualization has improved the understanding of the engineering problems.

As there is many research done in the field of FEA, AR, topology optimization and FEA-AR integration, it is possible to collect the researches in three topics: research on structural topology optimization and applications in automotive industry, FEA-AR integration and topology optimization in automotive industry.

2.1. Structural Topology Optimization

The structural topology optimization is concerned with increasing the utility of a certain quantity of resources to satisfy given objective. The selection of

the best structural design is performed based on the three categories: size, shape and topology optimization (Bendsoe et al., 2003). The research called “Limits of economy of material in frame structures” shows one of the first solution in order to reveal the most suitable size and continuum by Michell (1904) in Figure 2.1.

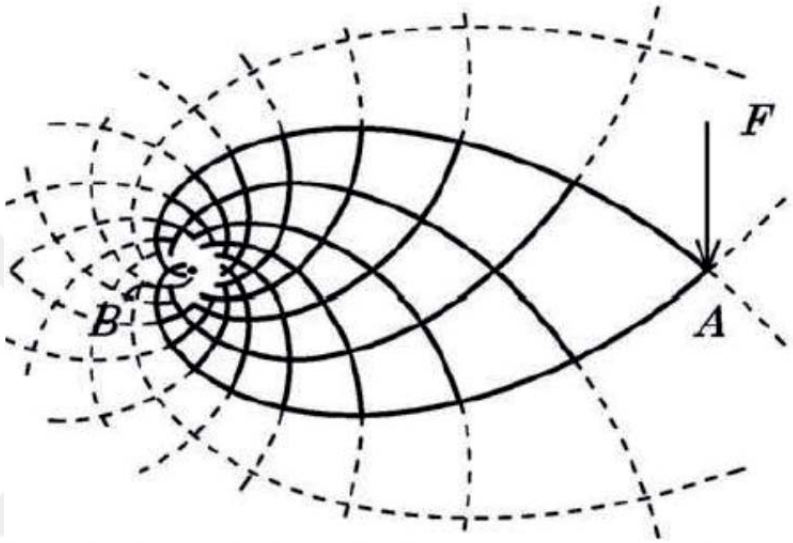


Figure 2.1. One of the earliest solutions proposed for the structural topology optimization problem (Mitchell, 1904).

More advanced techniques have been developed to tackle more complex problems. Engineers have managed to succeed weight savings in many structures as a result of the utilization of these advanced techniques. Kingman et al. (2015) have focused on the applications of topology optimization in structural engineering in particular to high-rise buildings and the steel components which are used when building them. They presented several buildings which were built/designed after the topology optimization in Figure 2.2.



Figure 2.2. (A) Office building in Japan, (B) Support structure optimized using TO and (C) A building in Doha using a support structure which is optimized using TO (Kingman et al., 2015).

In material science, structural topology optimization finds many applications as well as in civil engineering. Ha et al. (2019) has carried out research focusing on the usage of TO on three-dimensional woven materials. The base structure design represents the object that is to satisfy a quite restrictive topological constrain which is connected with three-dimensional weaving. Figure 2.3 demonstrates the initial pattern and the pattern obtained after topology optimization that corresponds to the constraints of the application.

Suzuki et al. (1991) has carried out research on TO of linear elastic plane structures to obtain the stiffest design using the homogenization method. Additionally, Duysinx et al. (1998), extended the research of TO techniques to the optimization of continuum structures with local-stress constraints. By using the outcomes of these research, Jung et al. in 2003 have carried out a TO of nonlinear structures by expressing effective stress and strain in terms of 2nd Piolar-Kirchoff stress tensor and Green-Lagrange strain tensor (Figure 2.4).

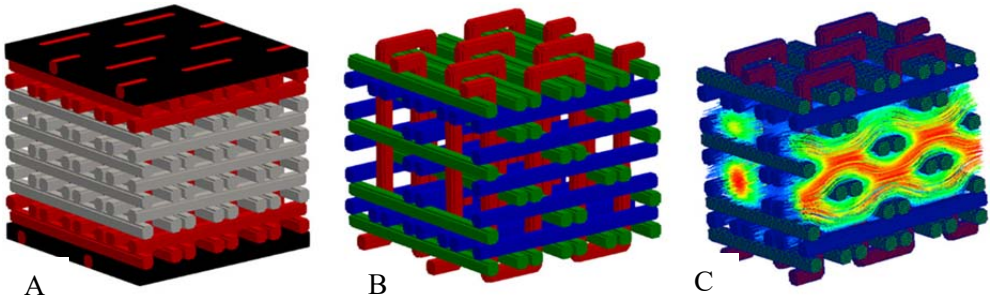


Figure 2.3. (A) The design domain sandwiched between black material to mimic the resultant structure when stacking and bonding of the lattices, (B) optimized lattice structure, (C) the optimized lattice structure that is sliced to reveal the fluid streamlines. (Ha et al., 2019)

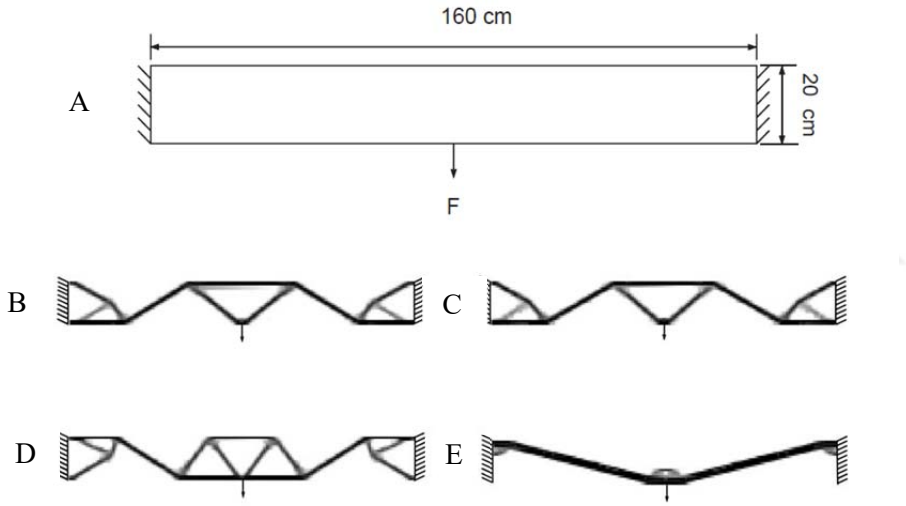
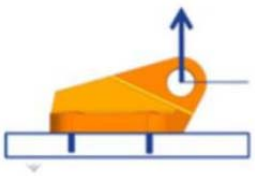
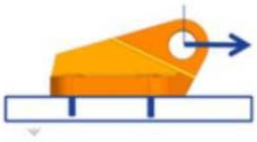
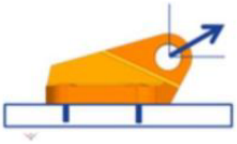
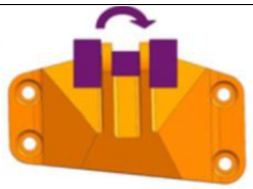


Figure 2.4. (A) A long slander beam which is subjected to F variable force (later in the research, this force is given as 10N, 15 N, 20 N and 30 N, optimal designs from (B) linear analysis, (C) materially non-linear analysis, (D) geometrically nonlinear analysis, (E) materially and geometrically nonlinear analysis (Suzuki et al., 1991).

Morgan et al. (2014) have finalized a design of a jet engine bracket and produced the designed part using additive manufacturing methods. The jet engine bracket was subjected to four different load cases as given in Table 2.1:

Table 2.1. Load cases specified for the jet engine bracket analysis (Morgan et al., 2014).

Load Case 1. **Static** **Vertical** **35586 N** 	**Load Case 2.** **Static** **Horizontal** **37810 N** 
Load Case 3. **Static** **42° from Vertical** **42258 N** 	**Load Case 4.** **Static Torsional** **Horiz. Plane at centreline of clevis** **565 N-m** 

Morgan et al. (2014) has carried out their topology analysis using Altair Optistruct 11.0. The first iteration condition was element density ≥ 0.3 and in the end the mass of the obtained first iteration design was only 8% of the original part. However, it did not satisfy the requirements as the stress levels were above the elastic limit (Figure 2.5). Second iteration included only 29% of weight reduction and the part satisfied the load requirements.

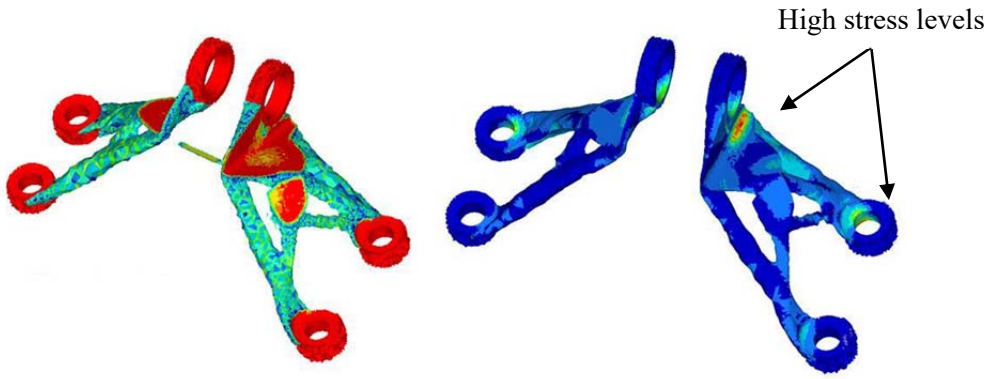


Figure 2.5. First iteration of TO done by Morgan et al. (2014).

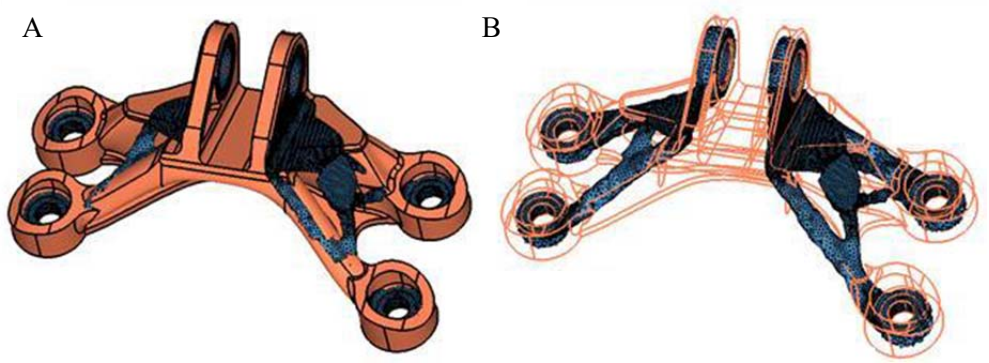


Figure 2.6. (A) Second iteration and (B) overlay of both iterations by Morgan et al. (2014).

2.2. Structural Topology Optimization Applications in Automotive Industry

The method of TO is becoming a "traditional" approach to optimization that aims at finding the best material distribution and therefore it is particularly effective in addressing structural problems that are solved with FEA. Weight reduction is a very recurring topic amongst the companies which are designing and producing high performance vehicles such as super cars or hyper cars. As the vehicle becomes lighter the performance and handling become much better. Therefore, having to carry less weight results in less fuel consumption, easier acceleration and better braking. However, the reduction of the vehicle weight comes with its trade-offs which includes safety performance in the event of any sort of collision. While decreasing the weight, engineers must not overlook at the safety factors of the obtained structures.

Many research started to appear in the field of automotive design and mechanics. One of them, Kilian et al. (2003) have addressed the optimization of hard drive suspension by increasing the torsion, bending and frequencies of sway mode (Figure 2.7.A). Chang et al. (2008) have used topology optimization to obtain an ideal geometry of a bracket of automotive air conditioning system where the bracket was used to support the compressor (Figure 2.7.B). The bracket was subjected to constraints of static loads and natural frequencies.

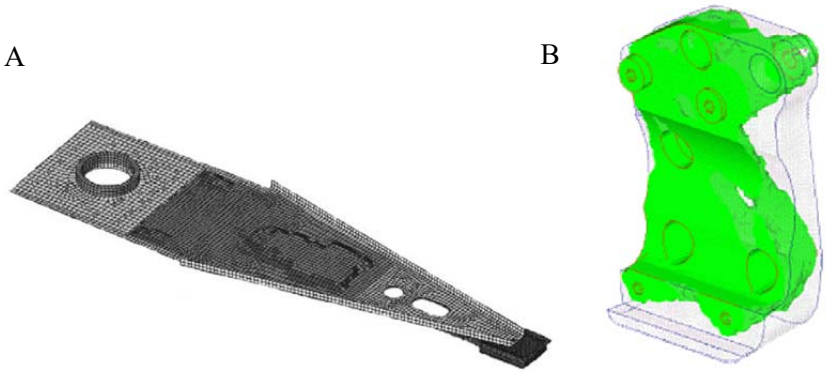


Figure 2.7. (A)Results of topology optimization of suspension by Kilian et al. (2003), (B) Results of topology optimization of a bracket by Chang et al. (2008).

Wang et al. (2004) have used TO methods to increase the stiffness of an automobile body by redistributing the material and optimizing the size. Additionally, Pedersen (2003 and 2004) have used TO in order to obtain an energy absorption history of a structure which is subjected to a crash.

Cavazzuti et al. (2010) have used TO method for the automotive chassis design to reduce the weight of the structure, match the performance requirements and safety requirements. Altair Optistruct 9 was used for the model setup and Altair HyperMesh 0 for the better calibration of the model and forces were defined as shown in Table 2.2. At the end of analysis, the topological model was not suitable for the manufacturing (Figure 2.8). The research employed a FEM code that set components which could be defined by the user. Following the obtained structure, the structure was enriched with beams that could be somewhat produced using extrusion process of manufacturing.

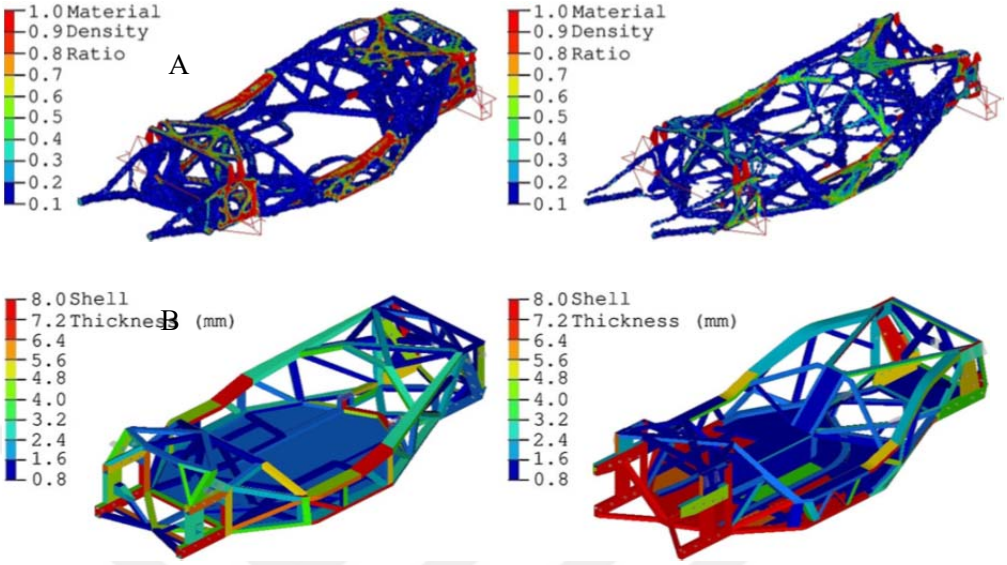
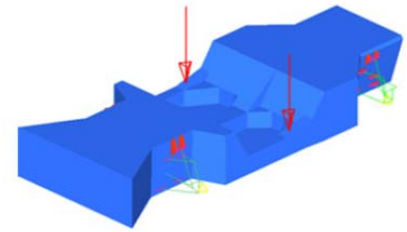
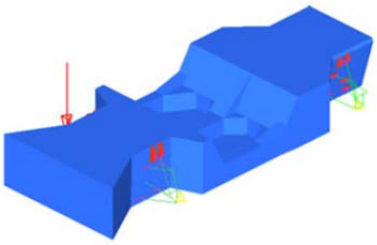
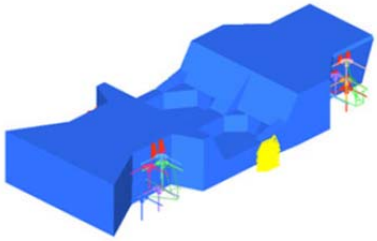
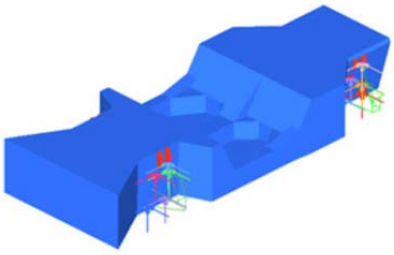
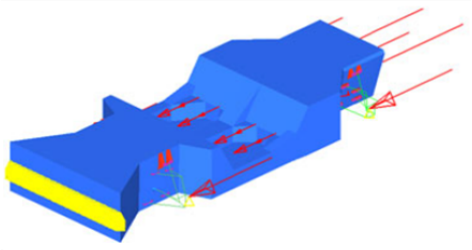


Figure 2.8. (A) Topology optimization results, (B) Size optimization with hypothetically manufacturable model (Cavazzuti et al., 2011).

Table 2.2. Loading configurations defined by Cavazzuti et al. (2010).

Bending stiffness loading configuration	
Torsional stiffness loading configuration	
Local stiffness with clamped sills loading configuration	
Local stiffness with inertia relief loading configuration	
Crash linearization loading configuration	

Cavazzuti et al. (2012) have handled a very similar optimization problem for Ferrari F430 concerning the chassis and the roof of the vehicle. The aim of the research was to present the results of the topometry and topology optimizations. The research showed that even though the results of this analysis did not deliver the final shape of the product, it gave useful hints for the designers on where to focus the density of the materials for the given structure (Figure 2.9).



Figure 2.9. (A) design space indicator, domain, (B) optimum configuration of the chassis, (C) optimum configuration of the roof (Cavazzuti et al. (2012).

Chiandussi et al. (2003) have presented their research on optimization of a vehicle's McPherson rear suspension subframe. Their method of optimization was to maximize the total potential energy with a volume constraint however the volume of the solution was not limited but was decided by displacements, stresses and stiffness values which were obtained after the FEA calculations. Figure 2.10 shows the forces, the rough shape of the rear suspension subframe and the forces applied in different scenarios.

The conclusion has been reached in two steps: the first step was to obtain a model that would be geometrically configured to a hypothetical producible shape and the second step was to bring the first proposed design to the final shape. Figure 2.11 shows the final shape of the suspension subframe which was analyzed by Chiandussi et al. (2003).

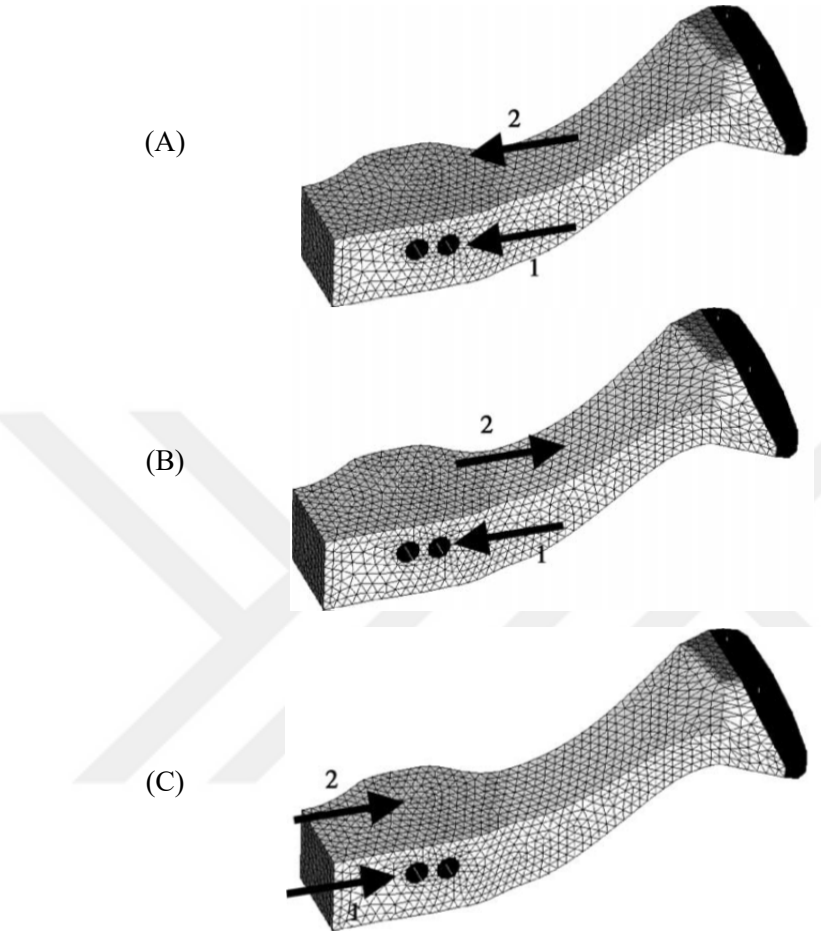


Figure 2.10. Forces (A) during steering, (B) during breaking, (C) when the suspension reaches its maximum stroke.

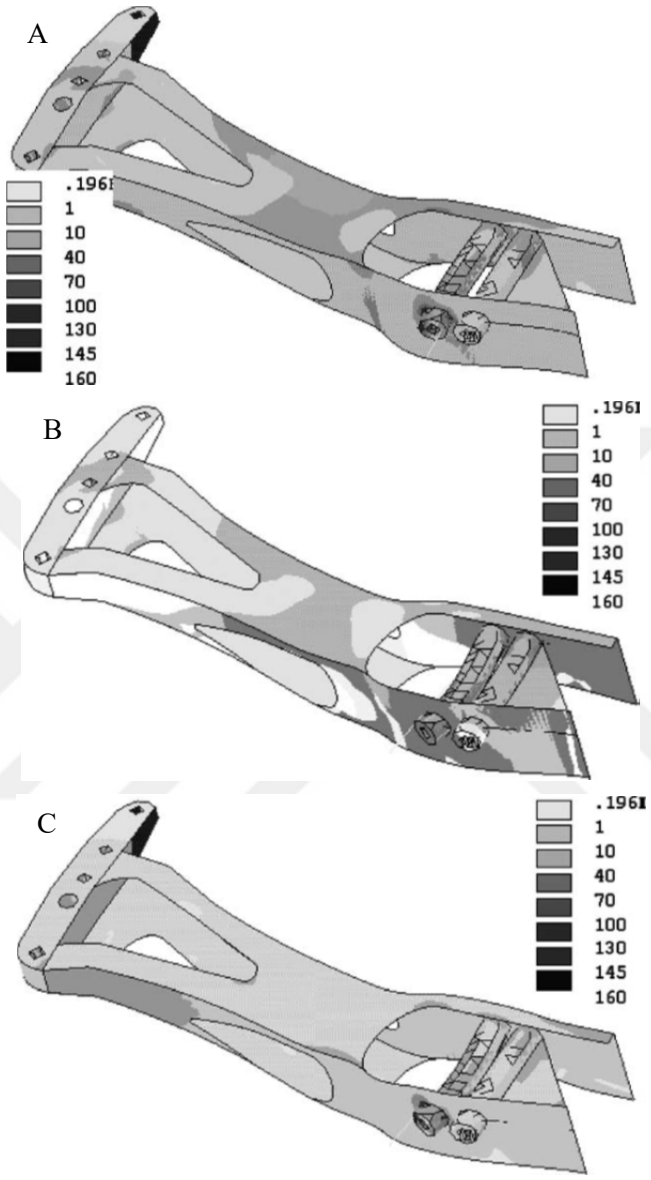


Figure 2.11. Final geometrical configuration of the rear suspension subframe analyzed for (A) during steering, (B) during breaking, (C) when the suspension reaches its maximum stroke (Chiandussi et al., 2003).

2.3. FEA-AR Integration

The first step of tackling an optimization process always starts with finite element analysis. FEA is used for identifying the weaknesses and strengths of the designed structures. While the FEA helps engineers to apply and test the scenarios in their virtual environment, the use of AR provides much more information about the design with an opportunity to visualize the FEA results on real components. This integration helps engineers to easily identify the critical areas and help better interpret the data.

Currently there are many research concluded with FEA and usually the representation of these results is viewed on the computer. Only few studies have been conducted on FEA-AR integration. Erkek et al. (2021) investigated an aluminum impeller which was used in pump that was used for energy transfer. The modal analysis of this impeller provided natural frequencies and the related deformation of the structure. Thereby, they used the results of their FEA analysis in a mobile FEA-AR based system (Figure 2.12).

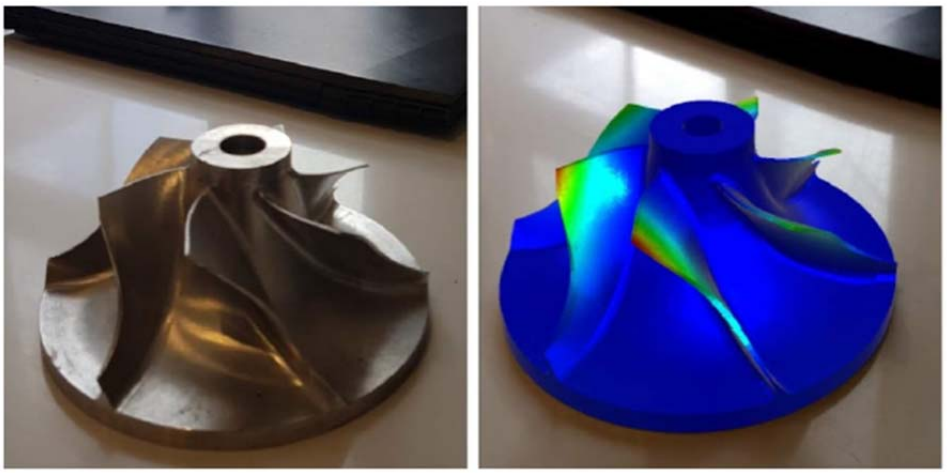


Figure 2.12. Product real-time view and AR visualization (Erkek et al., 2021).

In automotive industry, the advancement of the mobile devices such as smartphones and tablets are helping to accelerate the adoption of the AR technologies for various reasons such as maintenance, inspection in addition to CAD technology (De Sa et al., 1999; Abdul Halim et al., 2018).

Alabaster (2013) has presented use of AR Heads-up-Display (HUD) in the place where driver's visor is and in which the system is overlaying the video with function of smart devices such as GPS tracker, object orientation and graphic display[4].

Hyundai company has developed an AR application for their users so that they can access the important information regarding the vehicle without the need of a professional, by just using their smartphones or tablets as presented in Figure 2.13 (Samuely, 2015) [5].



Figure 2.13. Hyundai's AR application demonstration (Samuely, 2015).

Ferrari offered their Showroom App in 2015 (Figure 2.14) which was using 3D tracking technology and recognizing the cars in real world, providing

[4] https://www.computerworld.com/article/2498299/pioneer-launches-car-navigation-with-augmented-reality--heads-up-displays.html (accessed by June, 2022)

[5] https://www.marketingdive.com/ex/mobilemarketer/cms/news/software-technology/21686.html (accessed by June, 2022)

information in layers such as colors, shapes and technical information so that customer could build their own specifications for the cars that they would purchase. The usage of AR has developed in a different direction and became one of the marketing tools (Abdul Halim et al., 2018).



Figure 2.14. Ferrari's Showroom app (Abdul Halim et al., 2018).

In terms of automotive maintenance, AR technology has been found useful as its capacity of overlaying the information onto the real hardware and it can also include the information of how the maintenance procedures for that equipment are. One of the early usages of the AR for maintenance purpose was presented by Fredrich (2002). Following this research, many companies from automotive and aerospace industry joined the project that makes use of head mounted displays (HMD), user interface and markers that help solving the problem. Dini et al. (2015) presented an AR technique using special goggles and wireless connected access in order to support the maintenance work for relatively complex technical innovations and services for the vehicles. The work was based on a BMW 7-series engine. While the tracking system was working, the AR based system was able to recover from the failures automatically.

3. MATERIAL AND METHOD

In this study, the aim is to design a front unit shock absorber for an automobile that will withstand to the given forces and will comply the packaging requirements by using TO method and AR visualisation to achieve more reliable results. The complete process will be given in 3 steps and each step will have their own sub-steps.

Suspension design, the first step, can not be finalized with a straigth-forward approach by just having the necessary dimensions. There are many variables that are needed to be taken into account such as type of suspension system, weight of the car, packaging requirements, weight/material, dynamics and finally the cost. The final design is achieved after completion of many stages: definition of the size, optimization of the parts while matching the cost requirements, acceptance of the final design and test builds. After the special test pieces are built, the following procedure is the ride-work where the actual product is mounted on the vehicle and the vehicle is subjected to various driving conditions. After the ride-work (in some cases), the final core components(i.e. valving, piston, rebound system etc.) and modular components (i.e. suspension spring, bumper, top mount and dirt shield etc.) can be decided. However, in some cases it is necessary to repeat the ride-work with new components. With the customer's approval, the design and bill of materials (BOM) structure can be finalized.

During the design phases, each and every component is selected after through several different types of analysis and testing results that provides several critical diagrams such as Damping force – Path and Damping force – Speed diagrams (i.e. Figure 3.1). For instance, each valving system is not subjected to FEA analysis but there are certain criteria that help engineers decide. After the initial decision, the damper is subjected to internal tests to see if the damping forces are matching with the intended values.

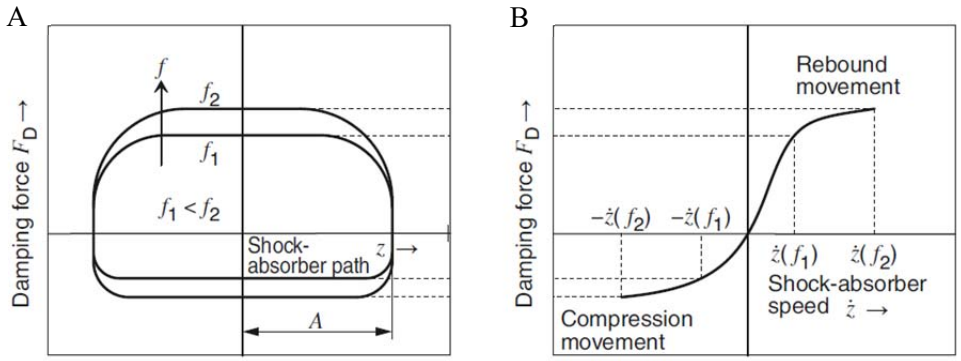


Figure 3.1. (A) Damping force – path diagram (B) damping force – speed diagram (Dietsche et al. 2022).

FEA is performed usually on non-core components such as pressure tube, yoke and rod in order to determine the optimal structure during the design phase of a shock absorber whether the decided components will withstand the defined constraints. Some of the components such as rod and reserve tubes already contain well-defined parameters and the behaviour of those components are well known. However, given load data and results might effect the size selection of those components. Therefore, those components are always included into FEA during the optimization analysis.

The design process is generally completed after obtaining the optimum structures and defining the components of the shock absorber. In this thesis, one more step is added to the procedure which is AR integration. With this step, it is aimed to achive much better decision making process and having to build fewer test samples in order to avoid additional production costs as any geometrical changes will result in significant cost increases.

3.1. Shock Absorber Design and Yoke Optimization

Defining the specification of a shock absorber can be extremely complex, covering the entire dimensional data, plus material specifications, manufacturing methods, oil and gas specifications and pressurisation as well as performance

specifications with tolerances. Essentially, the shock absorber must be connected to the vehicle and bear the forces that it is designed for. Therefore the main specification features are considered to be:

- fitting to the vehicle
- rod travel distance
- characteristics (damping force – path and damping force – speed (Figure 3.1))

The functional specification may be achieved in several ways, but to assure the performance over the defined conditions, following items are taken into consideration:

- configuration (tuning)
- rod-pressure tube combination (also known as rod-bore combination)
- oil and gas properties

When it comes to the life of a damper, it is defined by the wear rate and maintenance of an acceptable damping force characteristics over the specified period of use. Durability tests, both pre-serial production and field(ride works), are required in order to finalize the dimensions and core components that gives the vehicle desired characteristics. To help to achieve durability, followings items highly contribute and are taken into consideration:

- seals
- surface finish
- contamination and corrosion resistance

According to requirements, for each individual case, other technical details may be added. Finally, last but certainly not least is the cost.

In most cases, engineers receive a quarter or half model of the vehicle including the neighboring elements that a shock absorber is connected to and others that shock absorber might get in contact if the packaging rules aren't followed. Figure 3.2 demonstrates basic two types of suspension style that designers receive from the requestors. Figure 3.3 shows a rare case where the shock absorber designers receive the packaging in too much detail. Additonally, in some cases designers receive the 3D packaging requirements of the vehicle in a swept form of moving elements without any significant details.

The received quarter or half model of the vehicle gives the information of what type of mounting will be used, rod travel distance and fracture of information about the rod-bore combination. Most of the companies, including Tenneco Poland, have their own standardized components that will cover a wide range of requirements. The selection of the rod-bore combination is achieved after side load analysis. By analyzing the piercing points defined by customer, side load information is achieved. For double wishbone mechanicsms, it is possible to define the piercing points such as: wheel center, lower ball joint, upper ball joint, outer tie rod ball joint, tension strut bush, lower control arm (LCA) bush, upper control arm (UCA) front and rear bush, topmount pivot point, shock lower bush, spring upper and spring lower. As a result of side load analysis, rod-bore combination is decided.



Figure 3.2. McPherson and double-wishbone type suspension elements(Arikere et al., 2010).

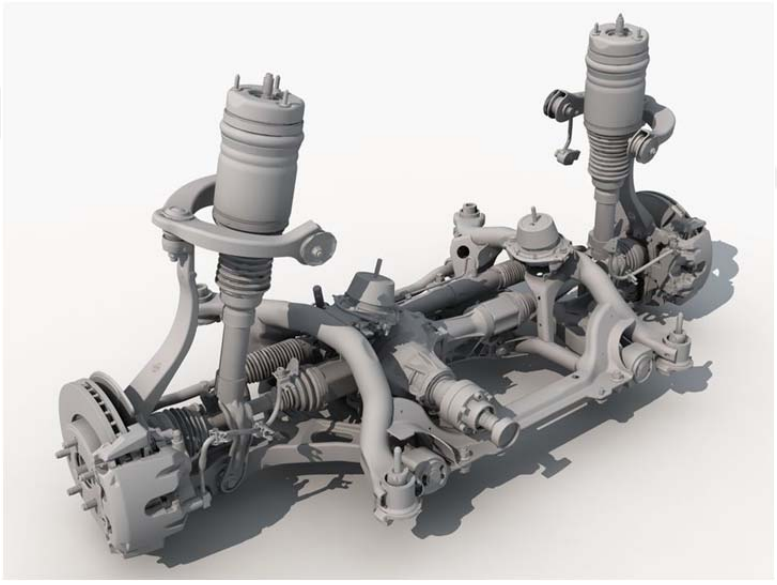


Figure 3.3. 3D model of a vehicle's suspension components that designers rarely receive from requestors[6].

[6] https://free3d.com/3d-model/front-suspension-8677.html (accessed by June, 2022)

Packaging evaluation contains most of the information that the designer needs such as: design length, compressed length, extended length, suspension kinematics, connection type such as loop-loop design or loop-top mount (for rear) or yoke (for front). With the given packaging and requirement file which is received from the customer, it was possible to obtain following information on Table 3.1. Additionally, the packaging gives information on how the product will be mounted on the vehicle. In most cases front units are mounted as a full module(strut) and rear modules with separate spring. Some customers request to have their producs as only the base which is shock absorber (Figure 3.4).

Table 3.1. Design requirements of a shock absorber.

Name	**Parameter/Type**
Shock level Design Length (DL)	687.3 mm
Shock level compressed length (CL)	624 mm
Shock level extended length (EL)	741.2 mm
Modular level DL	692.5 mm
Modular level CL	644.2 mm
Modular level EL	750.9 mm
DL load	8 kN
EL load	1 kN
CL load	36 kN
Top mounting	Front strut top mount
Bottom mounting	Yoke, without bushing
Type of shock absorber	Coil-over - monotube



Figure 3.4. Module (also known as “strut”) vs Shock absorber.

The characteristics are defined by the selection of the valve components. With the selection of valving, the pressure and forces that are acting on the shock absorber can be controlled. Selection of the valving defines the damper forces which can be represented by:

$$F_{damper} = \Delta p(A_{tube} - A_{rod}) + p_{gas}A_{rod} + F_{friction} = F_{damping} + F_{gas} + F_{friction} \quad (3.1)$$

where:

Δp = pressure drop over piston (Pa)

A_{tube} = section of the pressure tube (m^2)

A_{rod} = section of the rod (m^2)

p_{gas} = gas pressure (Pa)

$F_{friction}$ = force generated by friction (N)

F_{gas} = gas force (N)

F_{damper} = force generated by damper (N)

$F_{damping}$ = damping force (N)

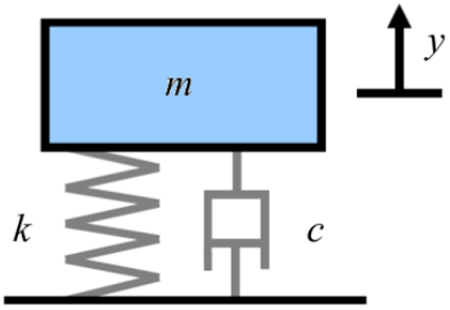


Figure 3.5. Shock absorber quarter-car modelling[7].

The quarter car shock absorber model (Figure 3.5) equation is given as following:

$$\ddot{y} + \frac{c}{m}\dot{y} + \frac{k}{m} = 0 \qquad (3.2)$$

where:

m = sprung mass (kg)

c = damping coefficient (Ns/m)

k = spring rate (N/m)

Solving Eq. (3.2), three different conditions are obtained:

- Under damping: $c^2 < 4mk$ where $\Delta<0$
- Critical damping: $c^2 = 4mk$ where $\Delta=0$
- Over damping: $c^2 > 4mk$ where $\Delta>0$

Most car manufacturers, in most cases, aim to reach the critical damping condition. For the under damping condition, residual vibrations occur after the vehicle hits a bump and it can be very dangerous considering the steering and control over the car. Overdamping gives very stiff and sluggish characteristic where it will be a very uncomfortable ride in a passanger car. However, over damping provides a lot of grip on rougher roads which is why it is mainly preferred

[7] https://steemit.com/steemstem/@masterwu/modelling-car-suspension-with-ode-s-damped-free-oscillations-part-2 (accessed by June, 2022)

to have on race car suspensions. Given the condition, the initial selection of the suspension can be achieved. Next step to analyze is the mounting condition of the module where it will be more clear how much force will be required from the damper.

An independent suspension is usually mounted on a vehicle with an angle (Figure 3.6). The main condition of deciding the distance D1 is to have 90º or close to 90º angle to the lower wishbone during the fully compressed state of the damper. Therefore, force that is applied from the wheel will be equal to module's reaction force:

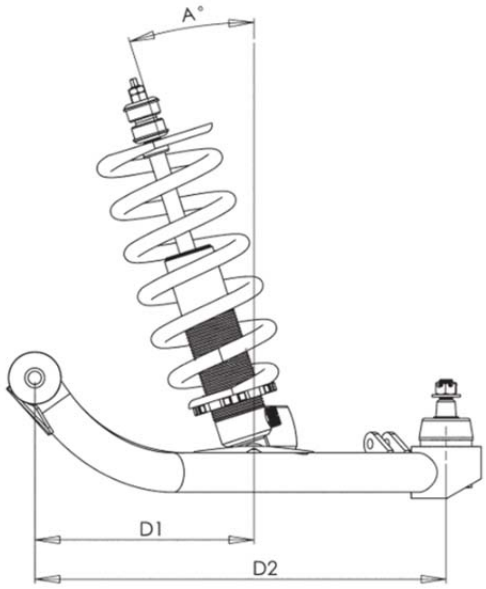


Figure 3.6. Module mountng angle and distance from lower wishbone pivot point.[8]

$$F_{wheel} = F_{module} \tag{3.3}$$

and therefore:

$$F_{module} = F_{damper} + F_{spring} \tag{3.4}$$

[8] https://www.qa1.net/tech-center/spring-rate-tech (accessed by June, 2022)

$$F_{spring} = k\,y \tag{3.5}$$

where y is an initial displacement of the spring.

According to the information provided by the customer, it is possible to determine the displacement of the rod and therefore determine the length of each component and module mounting points D1, D2 and angle A. Selection of the standardized components such as pressure tubes and rods are generally straight-forward given the circumstanses of the production size. There are standardized tubes and in terms of reliability and costs, it makes more sense to continue the design with a selection from the standards list. Rest of the components such as suspension spring, rebound system and valving is specially selected for the vehicle's characteristic requirements which are mentioned above. Therefore, there is one major component left to design and optimize, which is the yoke.

3.2. Design and Topology Optimization of the Yoke

As discussed in the previous section, the first step to tackle this optimization problem is to define the number of parameters which will be a decisive factor in optimizing the design shape. The general form for the TO problem can be described as:

$$\text{minimizing}_{p} \quad F = F(u(p),p) = \int_{\Omega} f(u(p),p)dV \tag{3.6}$$

$$\text{conditional with} \quad G_0(p) = \int_{\Omega} p dV - V_0 \leq 0 \qquad G_j(u(p),p) \leq 0 \text{ with } j = 1,\dots,n \tag{3.7}$$

Where the function $F(u(p),p)$ is an objective function which might differ for each individual problem but generally the equation with the aim of minimizing compliance and maximizing the stiffness can be used. Density is represented by p

which also refers to material distribution. The density is described between 1 and 0 where 1 represents the material and 0 represents empty areas. The linearity and nonlinearity is represented by u in this equation (Sigmund et al., 2013). The $u(p)$ is for design space and while determining this value, as mentioned before, many design factors are taken into account. Where n constraint is a characteristic that the solution must be satisfying $G_j(u(p), p) \leq 0$. For example, volume constraint (highest amount of material to be distributed) or maximum stress values.

Evaluation of the $u(p)$ requires solving the given differential equations (3.6 – 3.7) usually by using method of finite element since the equations do not have an analytical solution (Querin et al., 2017).

Next step is to apply the discussed methodology onto the real objects by first defining the volume limitation. Figure 3.7 represents the available packaging space and mounting points determined by measuring the nearby components. Some customers require minimum distance of 10mm or 15mm free distance between the shock absorber components and neigbour components such as body-in-white construction, steering knuckle, anti-rotation bar etc.

The length of the yoke is decided by other dimensional requirements such as DL, EL and CL of the entire module. According to the load requirements given in Table 3.1, and the valve setting evaluation tests, the gas pressure was decided to be 20 bar gauge and maximum damping force in compressed state was 1840 N. Therefore the rod diameter is decided to be Ø14 mm, pressure tube inner diameter to be Ø36 mm and reserve tube outer diameter to be Ø40 mm. After obtaining these values, designer can select the appropriate length of the shock absorber tube and therefore the height of the yoke is decided. The other dimensions are determined according tho CAD representation of the suspension design delivered by the customer.

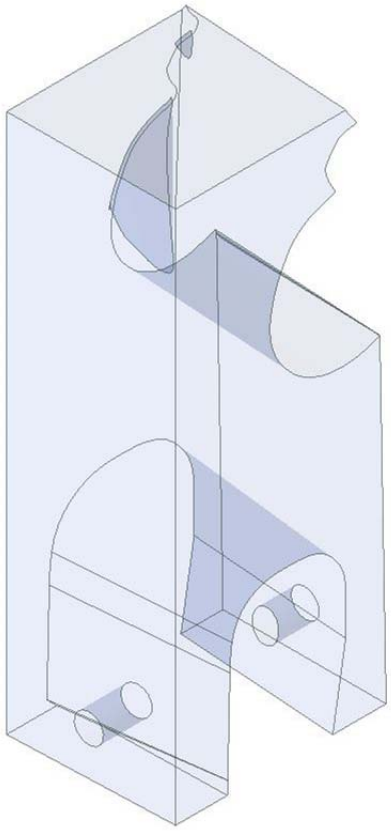


Figure 3.7. Available design space for shock absorber yoke.

Once the shock absorber tube is selected, it is possible to start the FEA analysis for topology optimization. In this thesis, analysis and optimization has been carried out by ANSYS Workbench Academic Student 2021 R2. Two different types of models have been created: one for topology optimization purposes (0) and other for validation of static strength analysis (Table 3.3).

Table 3.2. Topology optimization analysis finite elements.

Part	Finite element type
Yoke	C3D10
Shock absorber tube	C3D8I
Rod	B31
Ball joint with bolt and nut	B31 / MPC

Table 3.3. Static strength verification analysis finite elements.

Part	Finite element type
Yoke	C3D10 + M3D6
Shock absorber tube	C3D8I
Rod with piston	
Ball joint with bolt and nut	

3.3. Design Iteration - I

When performing the topology optimization of the given design space, following geometries presented in Figure 3.8 is obtained. The volume was first reduced by 60% and then by 70%. It is quite obvious that these shapes can be produced but it will not be very profitable and repeatable in high volumes. Therefore, after obtaining the first shapes a model based on the previous experience has been generated (Figure 3.9). This model is fitted in the given suspension elements and it complies with the packaging.

The first design that is presented in Figure 3.9 has a volume of 220.136 cm^3 and the weight of 2.512 kg. It is designed to work with the pressure tube that has a dimension of Ø36 mm and thickness of 2mm.

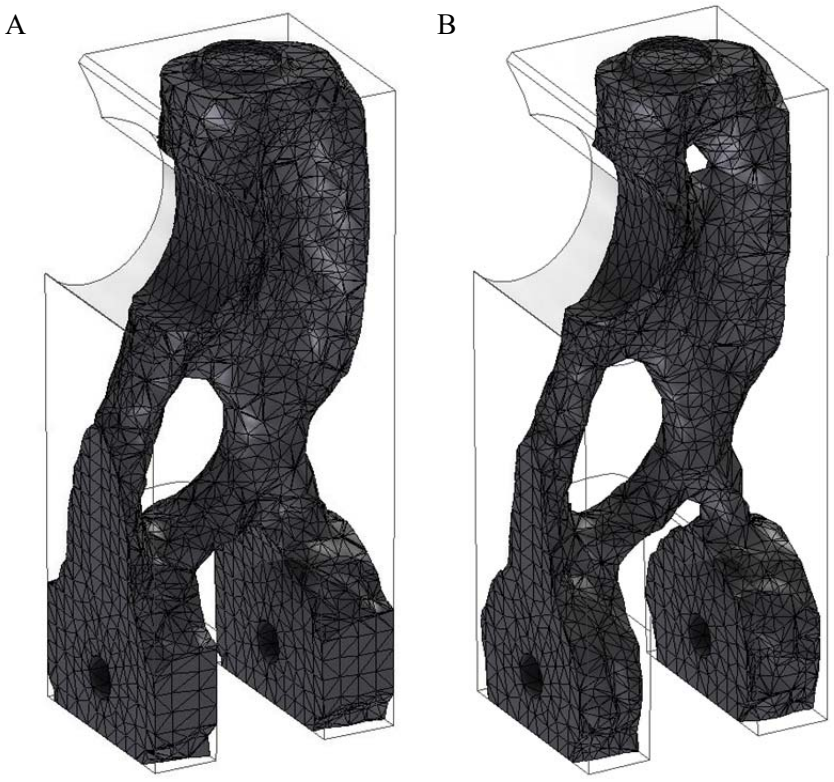


Figure 3.8. Topology analysis of the available packaging space with (A) 60% and (B) 70% volume reduction.

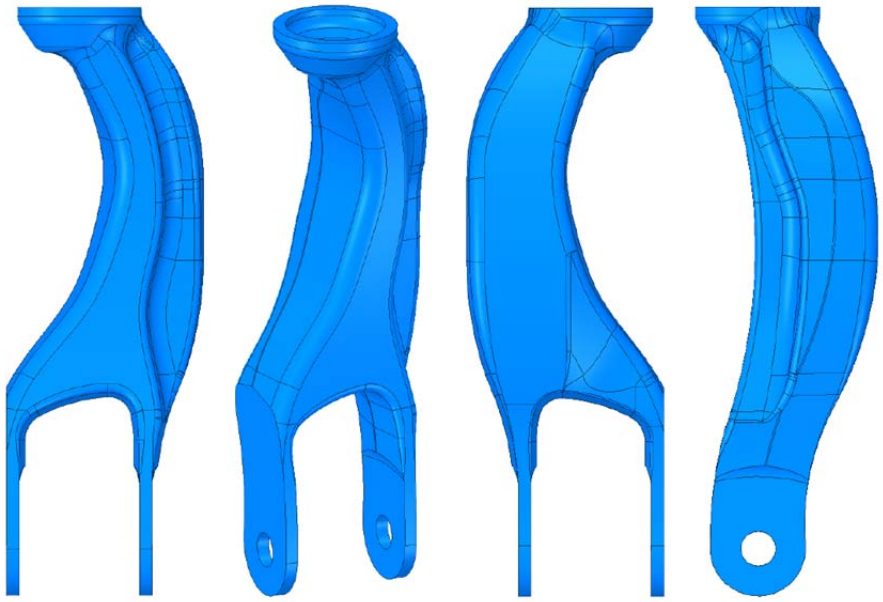


Figure 3.9. First concept design created by considering the output of the first topology optimization, based on packaging requirements and previous experience.

In order to carry out the analysis of this first iteration, tube, rod and ball joint with bolt and nut has been added to the assembly. Table 3.4 tabulates the properties of each material. However, several factors were not taken into account such as material strain hardening during manufacturing process and heterogeneity of stamped, forged and sintered parts.

Table 3.4. Material properties of the components.

Part	Material	Young Modulus [MPa]	Poisson ratio [-]	Yield strength [MPa]	Tensile strength [MPa	Elongation [%]
Yoke	38MnVS6*	210000	0.3	700	930	12
Pressure tube	E235+C**			400*	490*	10
Rod	EN 10083-2*			N/A		
Ball joint with bolt and nut						

* Please refer to the Appendix A-1 for the material information.
**Please refer to the Appendix A-2 for the material information.

Strength analysis were performed according to shock absorber CL position. EL position is usually not taken into account due to smaller forces. Axial loads have been applied to the area of the rod guide and according to customer requirements.

- F_1 = -83kN – allowed maximum permanent deformation is 0.2mm.
- F_2 = -91kN – no cracks or separation allowed.

In addition to the above loads, side loads from modular components have been added to the analysis:

- 476N lateral spring load
- 1.3Nm of lower bushing movement (X direction)
- 14.2Nm of top mount movement

35.2kN bolt pre-tension load has been applied which is a result of clamping the yoke. The value of the bolt load comes from tightening moment of 105Nm (max of 95Nm ± 10Nm on M14x1.5 load).

According to the results of the analysis, the given yoke geometry is not able to withstand the static compression loads that are specified by the customer. The reason for this is the plastic deformation of the tube. The dependency between yoke and tube plastic deformation is that one of the components deform plastically, the higher bending moment is generated due to the increase in eccentric vertical load. This leads to rapid development of plastic strain level in both parts and eventually causing the structure to lose stability. Eventually, it is suggested to increase the material grade of the tube. In addition, the weight reduction of the yoke was requested by the customer due to restrictions and performance requirements. Therefore, second design iteration has been carried out.

3.4. Design Iteration – II

For the second design iteration, the topology optimization process has been repeated but this time by using the existing design in the design iteration I. This topology optimization directs towards the correct reductions from the part. Additionally, the analysis has been carried out regarding two different location force requirements: China and Europe. These forces are defined as

- F_1^{EU} = -69kN / -76kN – allowed permanent deflection is max 0.2mm
- F_1^{CN} = -83kN /-91kN – no cracks or separation allowed

In Figure 3.10, the points of material reduction have been shown with arrows. However, the analysis results suggest to reduce the bottom of the yoke. This has been caused by carrying out the analysis only for the compression forces. As discussed before, forces in the extended length are much less in comparison with the compressed length, therefore, the analysis has been left at this point.

Moreover, it is mechanically not possible because carrying out this reduction will compromise the working principle of the yoke. Therefore, it is ignored in the future modification.



Figure 3.10. Second iteration topology optimization of the yoke and possible material reduction points.

New design proposal for the yoke (Figure 3.11) has reduced 1.58kg weight which is 37% of the initial design. Component cross-section (Figure 3.12) shows the locations where the material reduction and relocation has been performed. The pressure tube dimension has been kept the same but only material properties has been changed (Table 3.5) in order to eliminate the possible buckling of the pressure tube. Next round of analysis has been carried out with the same set of finite elements presented in Table 3.3.

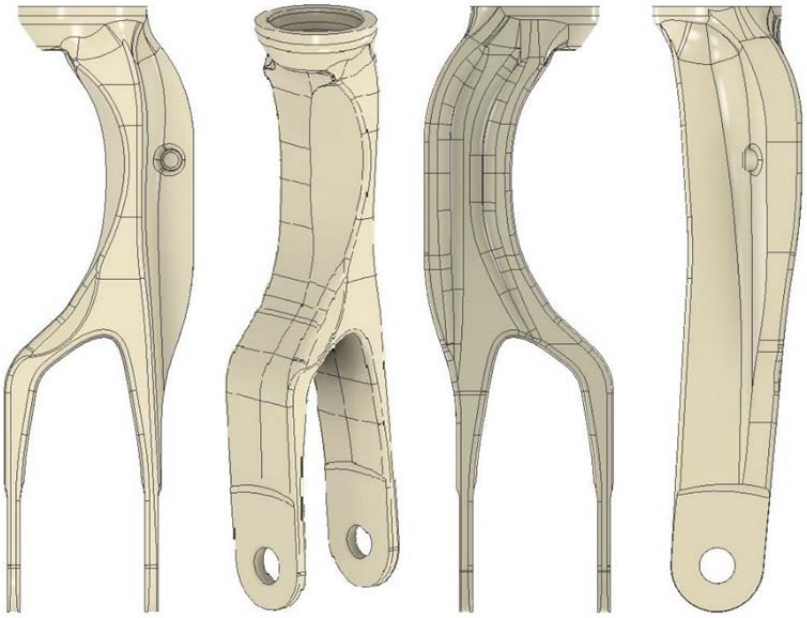


Figure 3.11. Second iteration of the yoke design.

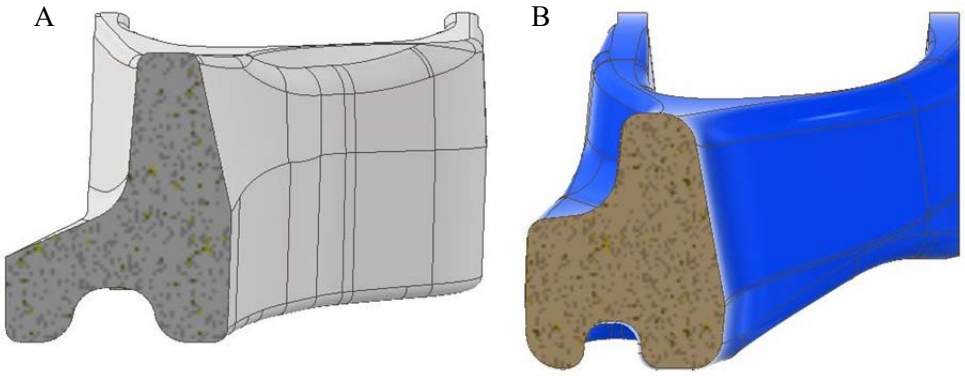


Figure 3.12. Cross section comparison of (A) second iteration and (B) first iteration yoke design.

Table 3.5. New material properties used in analysis

Part	Material	Young Modulus [MPa]	Poisson ratio [-]	Yield strength [MPa]	Tensile strength [MPa	Elongation [%]
Yoke	38MnVS6*	210000	0.3	700	930	12
Pressure tube	E335+C**			650*	700*	6
Rod	EN 10083-2			N/A		
Ball joint with bolt and nut						

* Please refer to the Appendix A-1 for the material information.
**Please refer to the Appendix A-2 for the material information.

According to the second design iteration results, the proposed combination of the pressure tube with E335+C material and new iteration of yoke withstands only 83.1kN force. The difference between the analyses of the first and the second iteration designs is that the forces are applied to the model with a 2 mm of misalignment in the second iteration as shown in Figure 3.13.

3.5. Design Iteration – III

Alongside the material strength and assuming yoke and tube dimensions, shock axial strength is dependent also on following factors:

- Clearance between yoke and ball joint and bolt pre-tension load
- Magnitude and direction of side loads
- Length of the shock and application point of spring load
- Geometry of welded connection between tube and yoke
- Bushings/joints characteristics

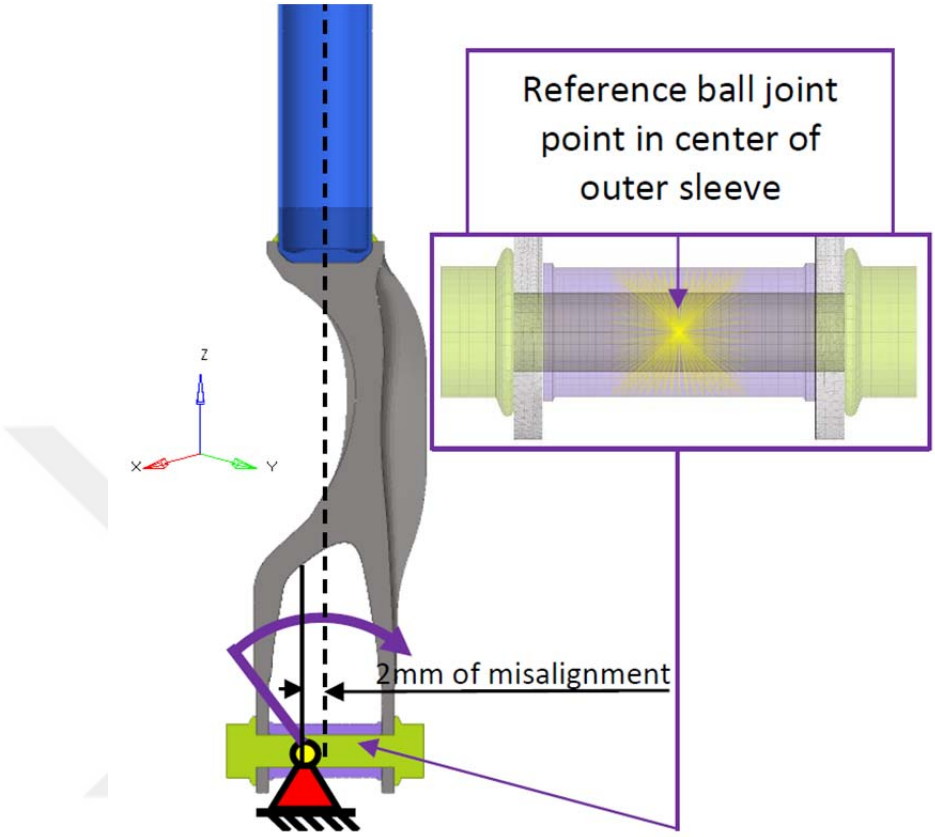


Figure 3.13. Load case with a misalignment of 2mm from the center of sleeve.

The objective of the third design iteration is to increase the strength of whole shock absorber by increasing the lateral stiffness of the yoke. This operation results in lower bending moment transferred to the tube due to eccentric compression and therefore to obtain higher axial load resistance.

As load and boundary conditions were kept the same as previous iteration, the difference is that the lower and upper fixation points. Values are represented in Table 3.6.

After applying the same load case setup and given requirements, it has been decided to design two different yokes for two different requirements (European and Chinese) of the shock absorbers. The reason behind this is that the

amount of material used in each yoke. According to analysis results, reducing the material from the design is going to compromise the stiffness of the yoke. Therefore, the decision was to produce two different yokes for two different requirements (Figure 3.14).

Table 3.6. Stiffness of lower bushing and top mount.

		Unit	Local X (damper axis)	Local Y	Local Z
Top mount stiffness	Translation	[N/mm]	587	565	565
	Rotation	[Nm/deg]	1.0	2.01	2.01
Lower bushing stiffness	Translation	[N/mm]	25000	25000	625
	Rotation	[Nm/deg]	5.0	5.0	1.125

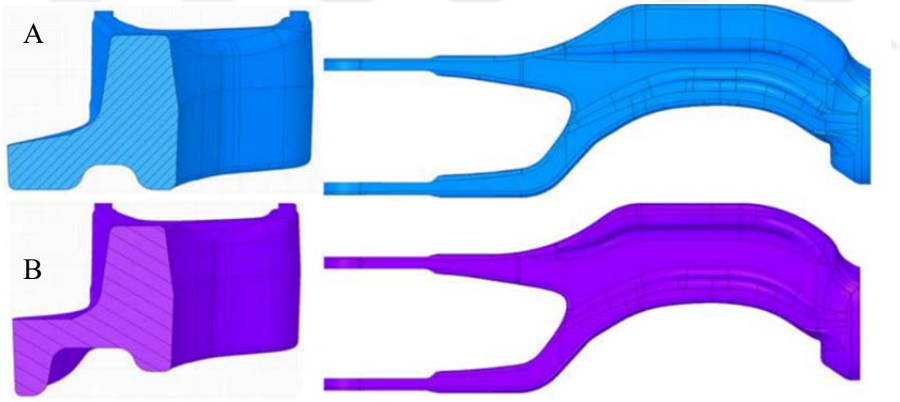


Figure 3.14. Yoke designed for (A) Chinese load cases and (B) European load cases.

3.6. Augmented Reality Implementation

The flow of developing an AR application consists of items which are presented in Figure 3.15: Exporting the desired 3D objects (complex or simple) to

create the guide lines for the recognition of the component geometry, exporting the generated guidelines and importing all information into the platform where model target detection will take place and finally building the application.

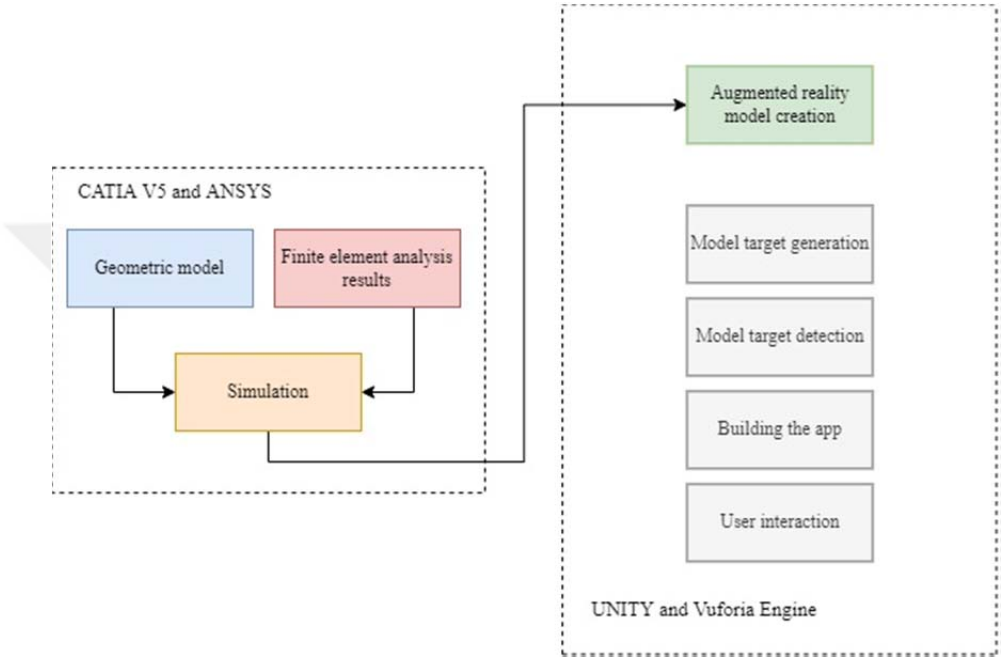


Figure 3.15. AR workflow and visualization of data.

As of 2022, there are many development platforms available to use for AR applications including the ones which are only specific to certain companies and not published for public use. Following platforms are the most commonly used for AR applications:

1. Unity by Microsoft
2. AR Core by Google
3. Vuforia Engine by PTC
4. Apple Arkit
5. EasyAR by Visionstar

6. Spark AR Studio by Facebook
7. Wikitude Augmented Reality SDK
8. Aryel
9. Bosch Common Augmented Reality Platform (CAP)
10. Amazon Sumerian
11. Holo|one sphere

In this thesis, Unity Hub with Vuforia Engine is used to create AR representation of the FEA results. Unity Hub is a platform where users can develop games and mobile applications that consists 2D and 3D graphic generation. It features real time graphics rendering engine, possibility of world-building, live operations analysis as well as reporting. It is also open to unite many different cross platforms and engines that can be imported for specific purposes. One of them which is Vuforia Engine which is widely used for creation of augmented reality applications.

Vuforia Engine is a software development kit (SDK) that helps creating augmented reality applications. With the help of Vuforia, it is possible to add an advanced vision functionality to the developed applications which allows recognition of images, objects as well as spaces with instinctual options to the created applications that enables real world interaction.

In order to work with Vuforia Engine, the asset must be imported into the Unity environment using Package Manager (Figure 3.16). After completing the import process, Vuforia Engine functions will be available. These functions include AR camera, image target, multi target and model target. In this study, AR Camera and Model Target options are used. AR Camera provides a perspective to the target object and helps define how the object is going to be viewed in the augmented environment. Model Target enables to build applications to recognize and track specified objects in the real world based on the defined way of viewing the object.

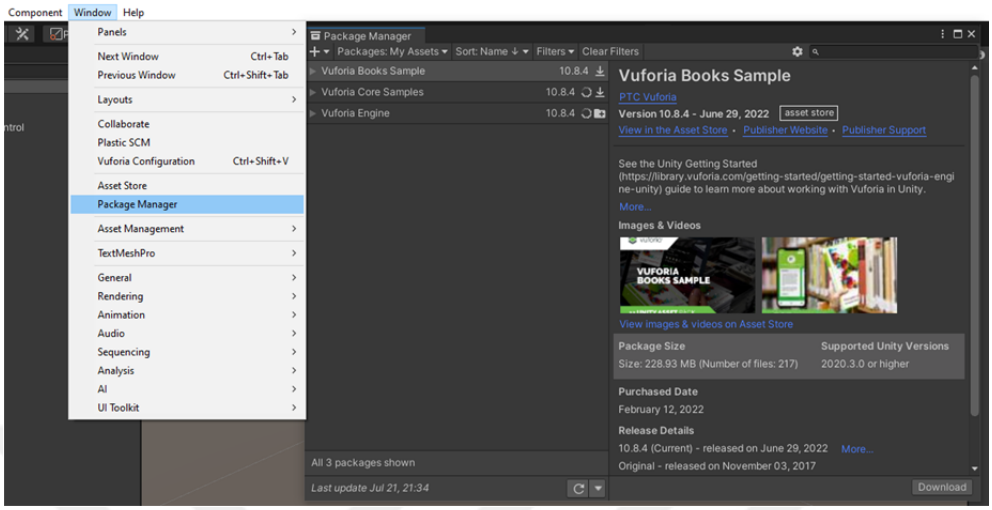


Figure 3.16. Importing Vuforia Engine in Unity using Package Manager.

Model Target Generator (MTG) is a tool which Vuforia provides to generate guidelines and necessary data set for an existing 3D CAD. The data set that is generated by MTG includes rendering of the model from the GuideView (detection position) which can be used to create a custom view image that will help better match the purpose of the usage (Figure 3.17). In the end of the MTG process, several files including custom viewpoints, 2D guideline and datasets for the Unity Editor will be obtained in file extensions of .dat, .unitypackage and .xml. These files contain information such as motion hint, tracking mode, entry point, rotation as well as translation. It is possible to generate model targets within Model Target Generator using files with various extensions that corresponds a 3D object such as .stp, .stl, .obj, .igs and .wrl.

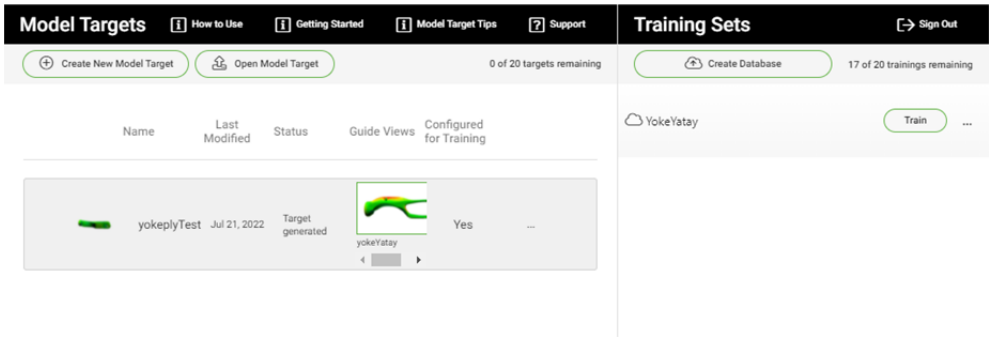


Figure 3.17. Model Target Generator interface.

Importing the results of the FEA results into the model target generator with the color shading requires several steps: first, the results must be viewed in ANSYS EnSight interface. This tool enables users to export the results of their analysis in various 3D formats such as .obj, .stl and .ply. Using this application, the results have been exported in .ply format that contains color, size and coordinate system information. However, it is not possible to import .ply files into Model Targe Generator tool. Other formats are not capable of keeping the color shading information therefore it is necessary to convert the .ply object into .obj using Microsoft 3D Builder application. As a result of this operation, along with a .obj file, a .mtl and a .png files will be exported. Importing the generated .obj file into Model Target Generator tool using the “Create New Model Target” button will result in visualizing the object with the color shading which is obtained after FEA (Figure 3.18).

First step of the generation is to decide the orientation of the object as a model target. All possible coordinate options have been given to the user within the tool. The most suitable way must be selected for the purpose of the application which in this case was Up Vector: Y option (Figure 3.19).

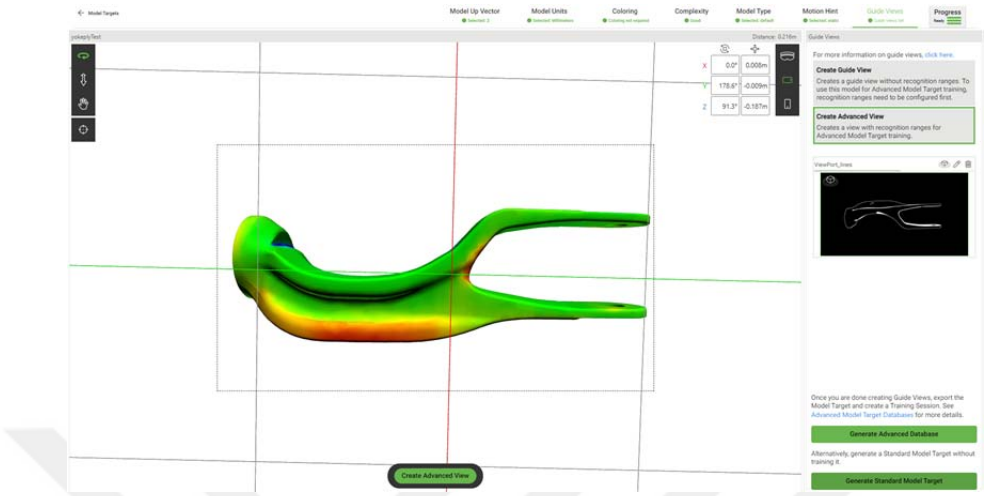


Figure 3.18. Importing the 3D object which is obtained after FEA results.

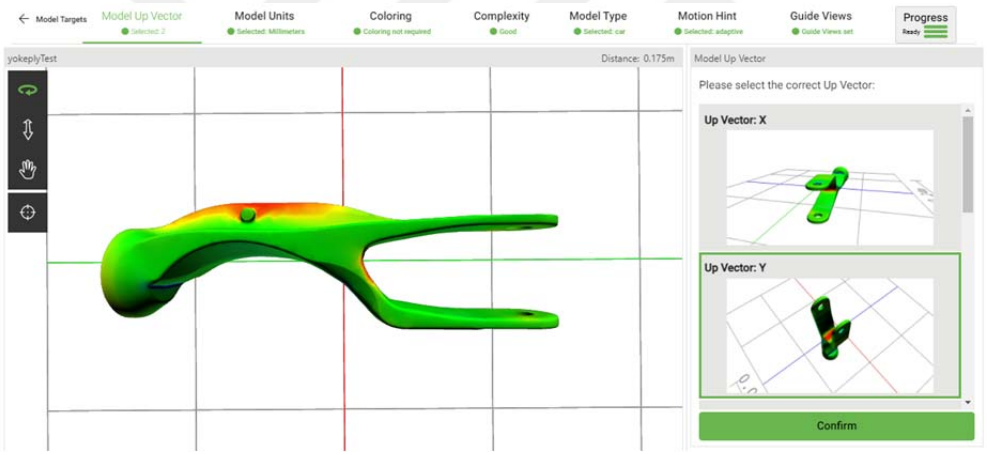


Figure 3.19. Model orientation selection prior to import of the object.

Next, the dimensional units of the object were selected which corresponds to the real object. In this case, exported unit corresponded to “meters”. Software then performs a check in terms of coloring and complexity. According to the information provided within the software, the more color and complexity given, the more accuracy of the model target is achieved. Next step is to select the model type that will the AR visualization of the imported model will correspond to (Figure

3.20). The option Default provides an object that does not have any reflective surfaces, option Car provides with a much more visuality to the component and option 3D Scan gives a texture of a 3D scanned object. In this study, the option Car was selected in order to reflect the colored surfaces with a much better interpretation.



Figure 3.20. Model Type options provided in the Model Target Generator software

One of most important steps is to determine the Motion Hint. This function assists the model tracking by what motion is expected from it such as static, adaptive and dynamic. Static option is used when the object is stationary. This option is selected in order to improve the tracking quality. Adaptive option provides motion hints of an object which may move during the AR experience. This option was selected in this study because the aimed visualization includes investigating the part in different point of views. Finally, the Dynamic option provides tracking of a constantly moving object (Figure 3.21).

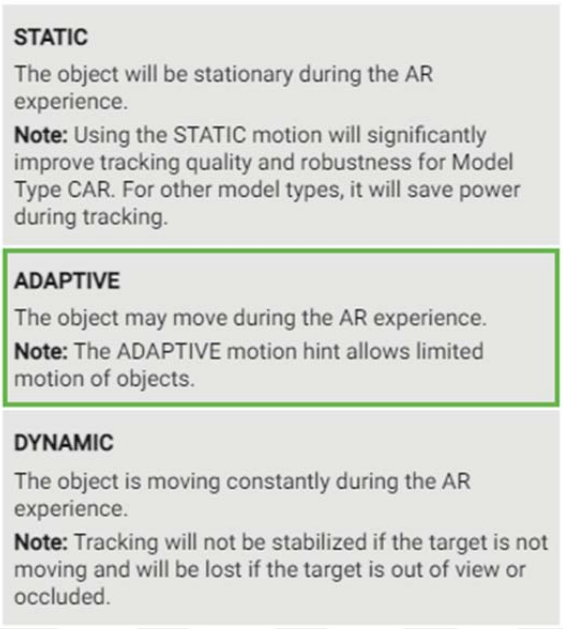


Figure 3.21. Motion hint options provided in Model Target Generator software

Final step of the model target generation is to decide the guide views. Within the Model Target Generator, user is given options to select on which device and which orientation the target generation will be completed. These options include Hololens, Landscape and Portrait concerning a mobile device. Then the recognition ranges are decided (Figure 3.22). There are two defined ranges: azimuth range (from -180º to 180º) and elevation range (from -90º to 90º). This function saves the model in defined rotations and later on it provides visualization of the object as the user starts rotating their device. Within the guide view step, the 2D recognition outlines (Figure 3.26) are created. Final step is to use "Generate Advance Database" button to create the necessary data sets for the Unity where the mobile application is going to be built.

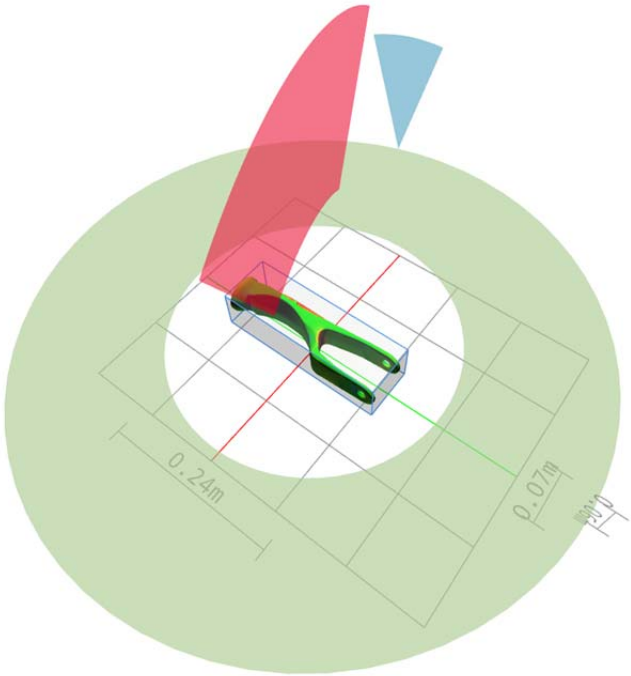


Figure 3.22. Recognition range selection within Model Target Generator software.

In order to start building the model target detection application, AR Camera and Model Target from Vuforia Engine needs to be added to Unity. In order to do that, steps within Unity has to be followed as: GameObject > Vuforia Engine > Model Target & AR Camera (Figure 3.23). After adding the assets, the file with .unitypackage extension then can be imported by drag&drop operation into any area of Unity. The object will look as shown in Figure 3.24. However, initially the object is shown with a single color. This will be corrected by importing the .obj file that consists .mtl and .png color shading information into the project folder and moving the object into the Model Target in Hierarchy panel on the left.

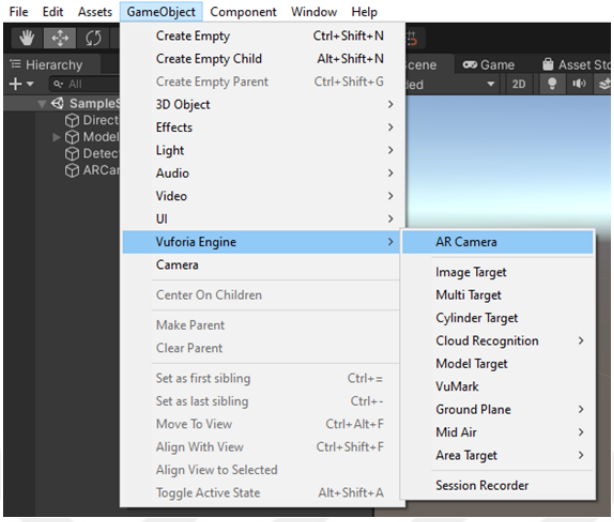
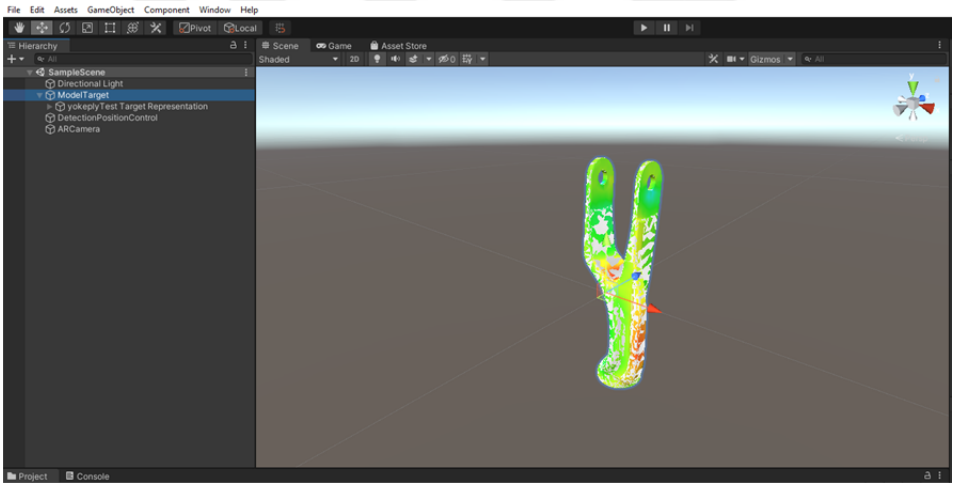


Figure 3.23. Importing Vuforia Engine assets to the Unity environment.


Figure 3.24. 3D data view after import as model target.

To be able to detect the correct material, the MTG software generates a guide view that matches the outline of the geometry in a specified angle. Completion of the setup is achieved by clicking the Model Target from Hierarchy window on the left which brings the panel on the right side of the window where user can find all available setup options (Figure 3.25). Within this window, user must select the guide view which was established in Model Target Generator. As a

default, Unity does not assign any guide views into the project. When the setup is completed, Unity will run the detection and look for a part that matches the given geometry. Figure 3.26 shows the moment where the camera of a device is activated.

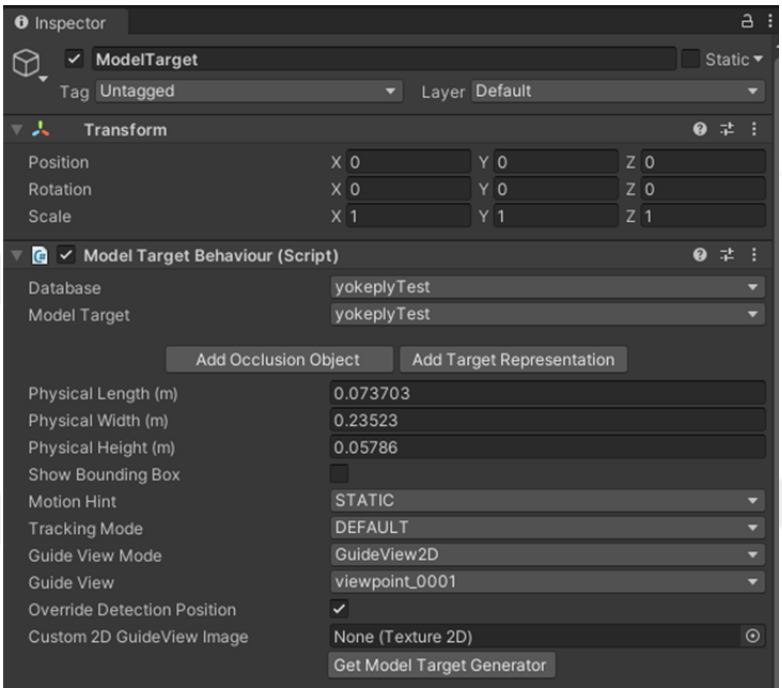


Figure 3.25. Model Target setup panel.

The last step is to deploy all the information on a device (preferably a mobile device which is operated by Android or iOS). This deployment can be done on different platforms such as PlayStation 4&5, WebGL, tvOS, Universal Windows and Xbox. During the preparation, user is able to select the platform that they will be deploying this application to.

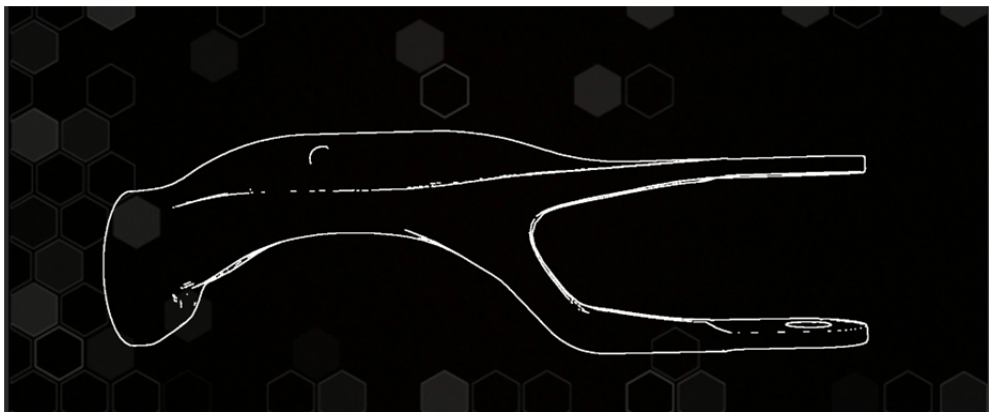


Figure 3.26. Generated 2D guide view.

As Android devices install the applications from files with .apk extensions, the Build Platform exports the necessary installation file to the given location. After exporting with the given settings, the application installs the app on the given Android device. The necessary requirement from the Android device is that it should be in Developer Mode. After entering the developer mode, USB debugging should be activated. The Android device is connected to the computer via USB and after the Build and Run command, all the information is transferred via USB connection (Figure 3.27).

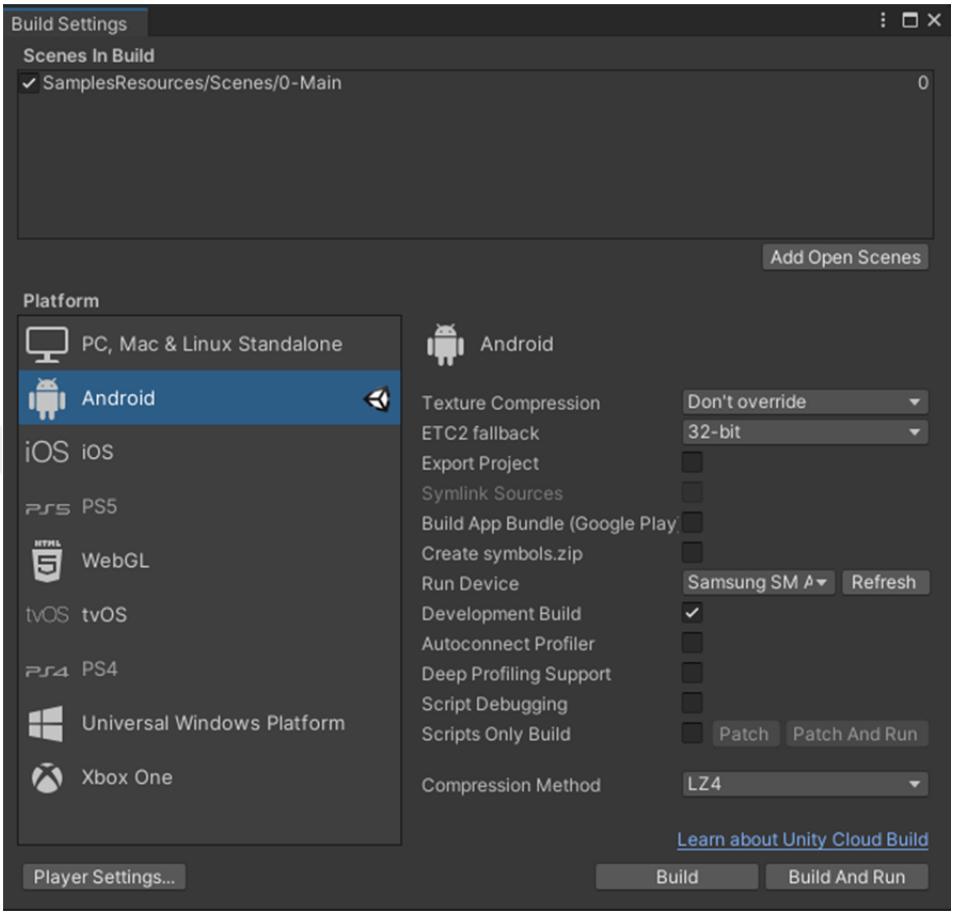


Figure 3.27. Build settings of Android and platform availability.

4. RESULTS AND DISCUSSION

4.1. Topology Optimization and Analysis Results

Three design iterations have been summarized in Figure 4.1. According to analysis results performed at Tenneco, Poland (Tenneco CAE analysis report #2952), shock absorber was not able to withstand the static compression loads specified by customer in the first design iteration. The yoke was able to fulfill the requirements in the second design iteration but high plastic deformations were observed on the reserve tube (Tenneco CAE analysis report #3048). Therefore, an upgrade for the reserve tube material was suggested. Third design iteration (Tenneco CAE analysis report #3455) was suggested such that given the two different loading conditions, it would be more beneficial to create two different yoke designs for each loading conditions (European and Chinese).

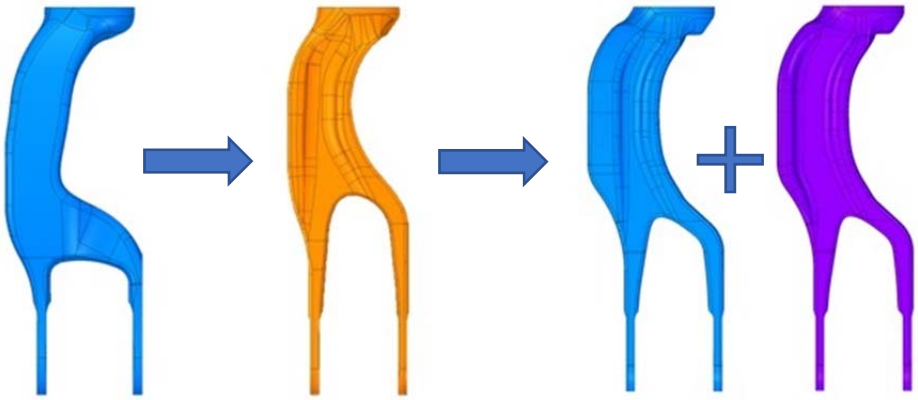


Figure 4.1. Summary of topology optimization results of three design iterations.

Analysis of the first yoke design has shown that combined axial and lateral loads together would result in significant drop in shock absorber's strength. Analysis results (Table 4.1) showed that given combination of tube and first yoke design was only able to withstand up to 84kN axial force which is below the required 91kN. Due to the dependency in terms of how the stresses are transmitted

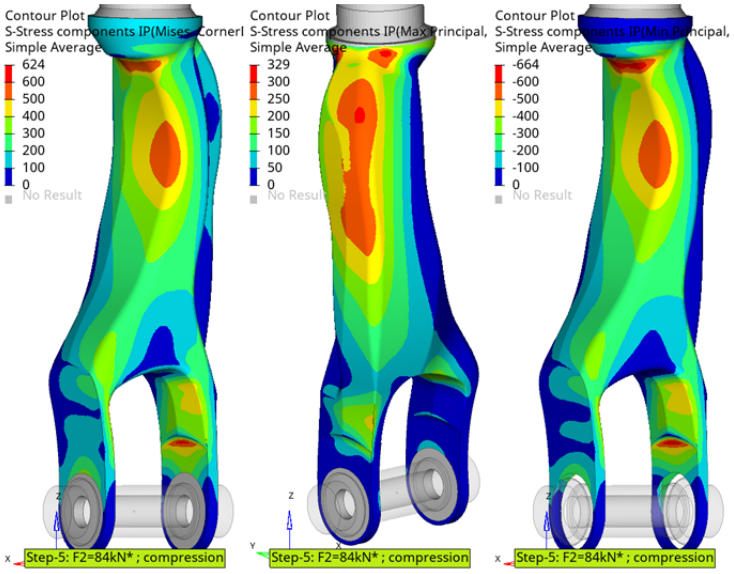
from yoke to pressure tube, pressure tube was observed to be subjected to 471 MPa Von Mises stress and therefore plastic deformation on the tube was observed (Figure 4.2).

Table 4.1. Stress-strain and deflection results for F_1 and F_2 load cases.

Result		**Unit**	**Assembly**	**F_1 = -83kN**	**F_2 = -84kN***
Yoke	Von Mises	[MPa]	258	617	624
	Max. principal	[MPa]	188	319	329
	Min principal	[MPa]	-281	-652	-664
	Equiv. plastic strain	[%]	0	0.00	0.00
Tube	Von Mises	[MPa]	0	470	471
	Max. principal	[MPa]	0	525	541
	Min principal	[MPa]	0	-553	-558
	Equiv. plastic strain	[%]	0	0.62	0.75

*-84kN was maximum achieved load while 91kN was required.

A



B

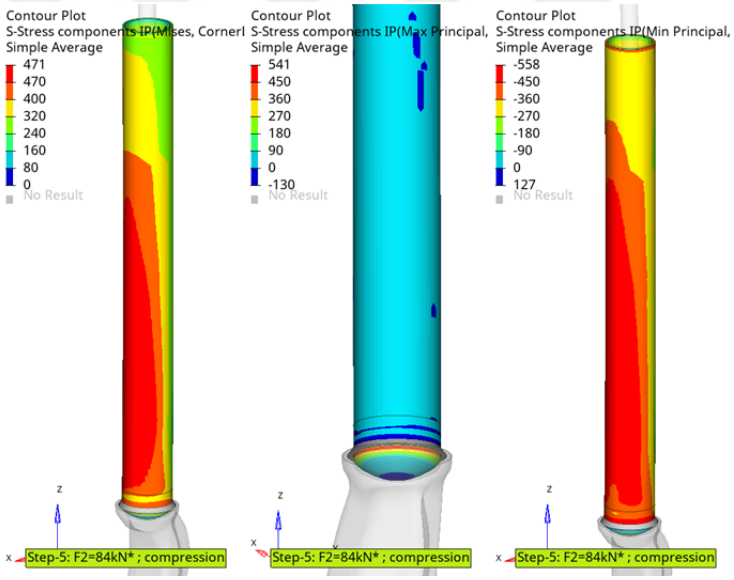


Figure 4.2. Von Mises, maximum and minimum principal stress [MPa] and equivalent plastic strain [-] distribution over (A) yoke and (B) tube under F_2 = 84kN (Tenneco CAE analysis report #2952).

The second design iteration analysis (Figure 4.3) shows that the new design of the yoke is able to withstand 17kN above the highest specified loading case which is the Chinese loading case of -91kN.

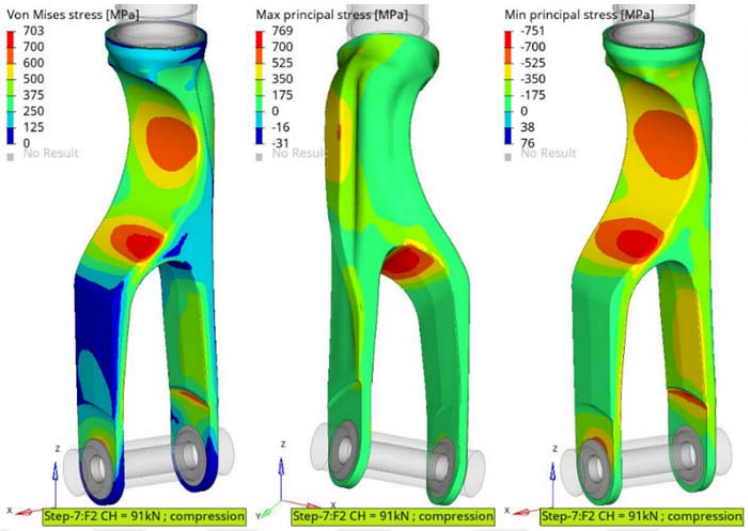
Comparing the pure-axial loading to combined axial and lateral loading together with misalignment of the lower mounting, reduction in shock absorber strength can be observed. In the cases, peak-to-peak comparison shows 12.0 kN of maximum loading capacity difference which is 10% of 120.4 kN vs 108.3 kN (axial only vs loads combination with misalignment (Figure 3.13)) (Tenneco CAE analysis report #3048). The strength analysis showed an increase by 27.6 kN and 31.4 kN respectively for combined axial -lateral loading. This is achieved by changing the tube material from E235+C to E355+C and higher stiffness of the yoke itself due to updated design.

Second design iteration was subjected to prototype builds. This prototype shock absorber has been tested to compare the FEA results with reality. In the second design iteration results, it can be seen that the tube is subjected to buckling forces due to mounting misalignment. In the prototype shock absorbers, same characteristics have been observed (Figure 4.4).

By performing the third design iteration analysis, the objective was to optimize and verify whether the new proposal of the yoke design could increase lateral (radial) stiffness. As a result of the optimization, two alternative yoke designs were proposed. Both yoke designs are 200 g heavier than the base design proposed in the second iteration. However, both designs increase the capacity of the shock absorber by 2.5 kN or 3.5 kN, depending on the material of the pressure tube.

At the beginning, the condition of permanent deflection was set to be maximum of 0.2 mm. Analysis results (Figure 4.5) has shown that yoke variant 1 with E235+C pressure tube subjected to European loads F_1EU = -69 kN and F_2EU = -76 kN resulted a permanent deflection of 0.016 mm and 0.018 mm. These values are acceptable according to initial requirements.

A



B

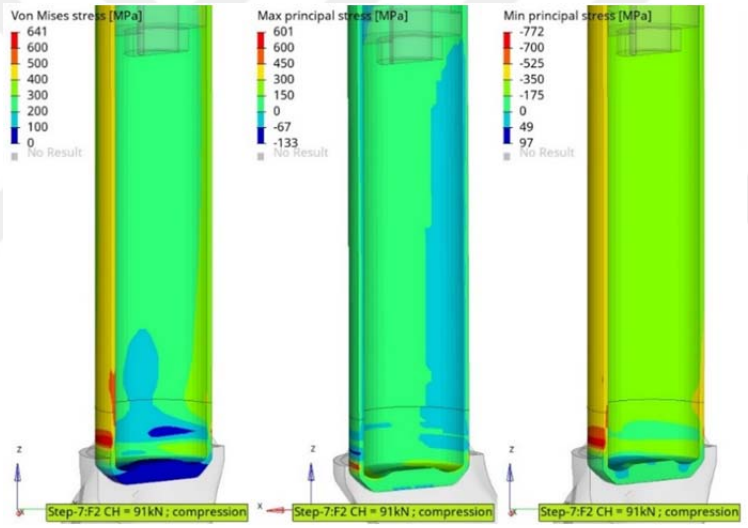


Figure 4.3. Yoke - Von Mises, maximum and minimum principal stress [MPa] and equivalent plastic strain [-] distribution over (A) yoke and (B) tube under F_2 = -91kN (Tenneco CAE analysis report #3048).

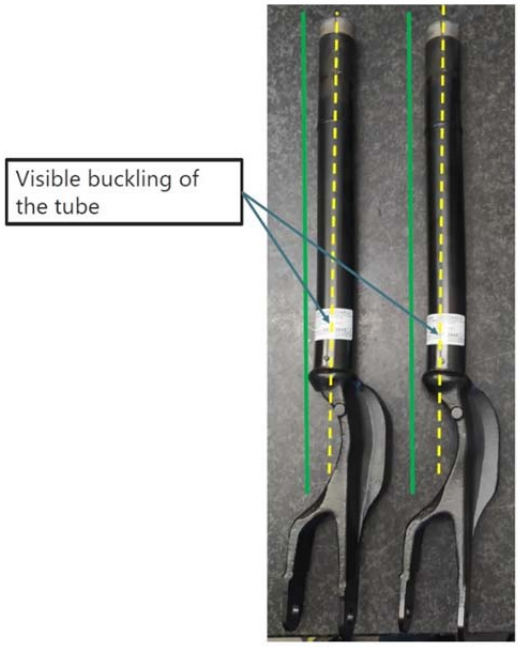


Figure 4.4. Visible buckling of the second design iteration prototype shock absorber.

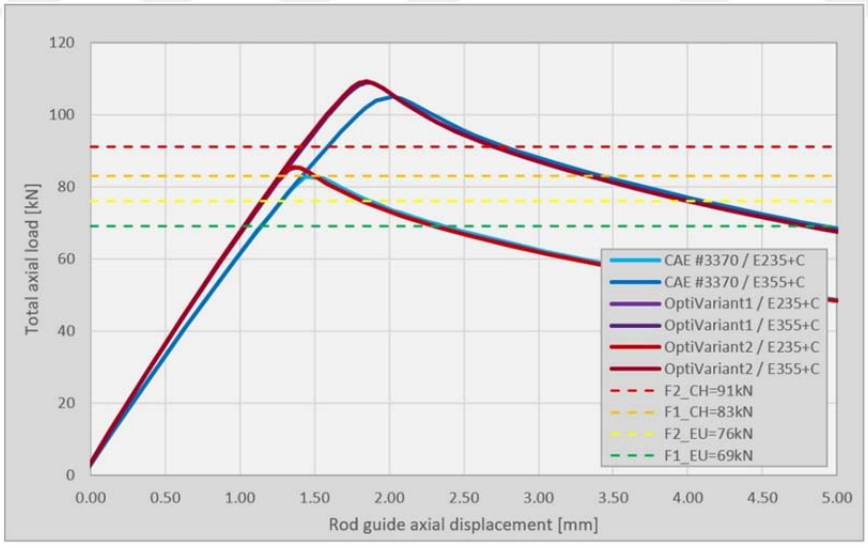


Figure 4.5. Load deflection graph for shock absorber which is equipped with two variants of yoke designs, 4 sets of load cases and misallignment.

Four different stress analysis are shown in all analysis results and accordingly, it is possible to see where the stresses are focused on Von mises stresses however due to the material properties of the yoke, the principal stresses give more detailed information on which part of the shock will be experiencing the stresses caused by the compression.

The results of the stress analysis of the first yoke variant with E235+C pressure tube under European loads is presented in Figure 4.6. The results show that according to the maximum and minimum principal stresses, the highest value of the normal stress (557 MPa) is in the middle (caused by assembling conditions) and the side of the yoke (caused by the compression forces trying to bend the yoke from outer side) and minimum value of normal stress is inside the right under the cavity, on the radius. By interpreting the Von Mises stresses, it is possible to see that yield points are represented quite similarly with the results of the minimum principal stress. The areas where the highest stresses are observed are due to the non-linear structure of the yoke. The Figure 4.6.B presents the possible buckling on the pressure tube. The stresses are focused on the inner side of the yoke and where the welding point is.

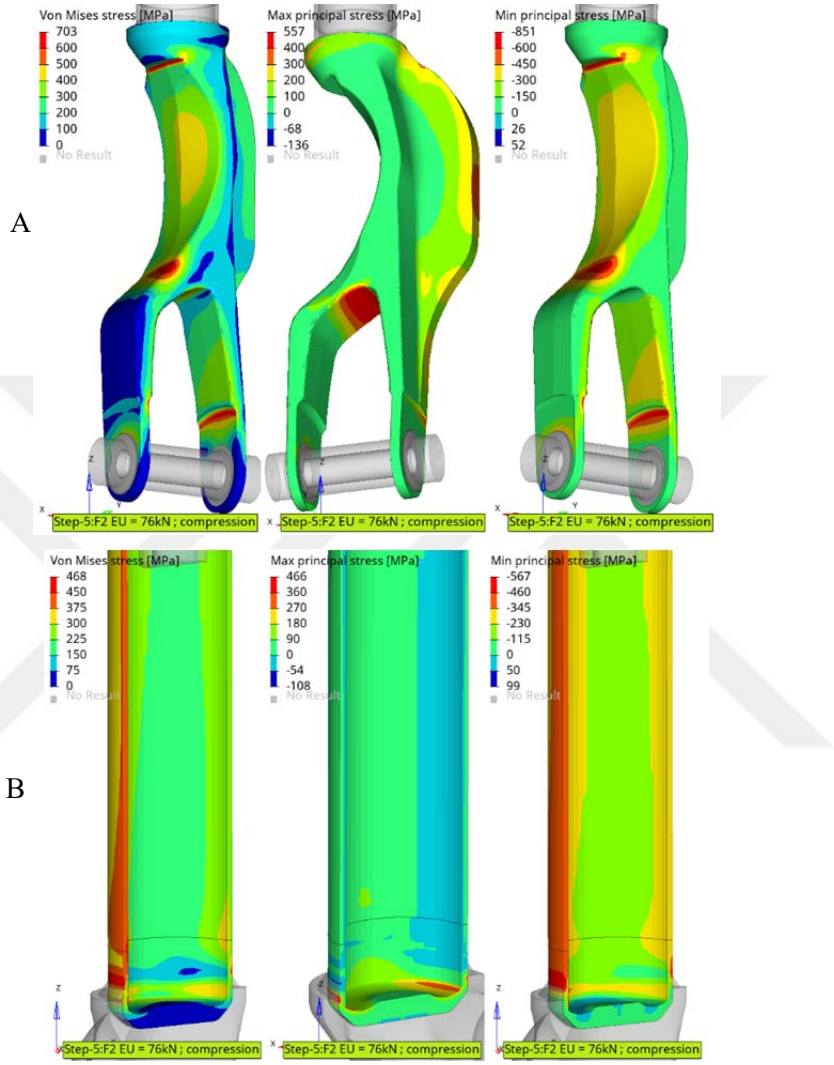


Figure 4.6. Analysis results for (A) yoke variant 1 with (B) E235+C tube. Misalignment with maximum EU load case (Tenneco CAE analysis report #3455).

The same variant with Chinese loading cases (Figure 4.7) has shown a deflection of 0.24mm on the pressure tube. This is still acceptable but at 85.3kN (see Figure 4.5), the pressure tube starts to deflect more than 0.2mm which exceeds

the initial requirements. Figure 4.7.B shows the focus of the stresses on the pressure tube. Even though the stresses which are acting on the yoke are very similar with the European loading case of the Varian 1, the results of the Chinese loading case with the same variant showcases a worse scenario for the pressure tube. The only difference between the yoke analysis results is that the area above the mounting point (see marked areas) where the stresses are shown is slightly bigger.

The cases considered above has featured the pressure tube with the material E235+C which was already proven to be weak for the Chinese loading cases. Therefore, analysis has been carried out with the new material E335+C which has a higher stiffness value. Therefore, big difference between the FEA results can be seen (Figure 4.8). Even though the force is higher than the earlier analysis (91kN Chinese), the yoke analysis results slightly resemble the previous one where the applied force is 83kN. The difference can be spotted in the pressure tube analysis results where the only stress focus area is the welding point. Even though the misalignment causes pressure tube to deflect more, the permanent deflection is found to be below 0.02mm.

The moment at which shock absorber starts to buckle (due to plastic deformation) is very similar for yoke variant 1 and 2. Based on the load-deflection curve (Figure 4.5), it can be easily seen that both the stiffness and the strength values are increased after the shape optimization of the yoke.

Based on the analysis results (Figure 4.6) it is safe to conclude that the yoke variant 1 with E235+C pressure tube can be used for production of the units that will be used according to European loading cases.

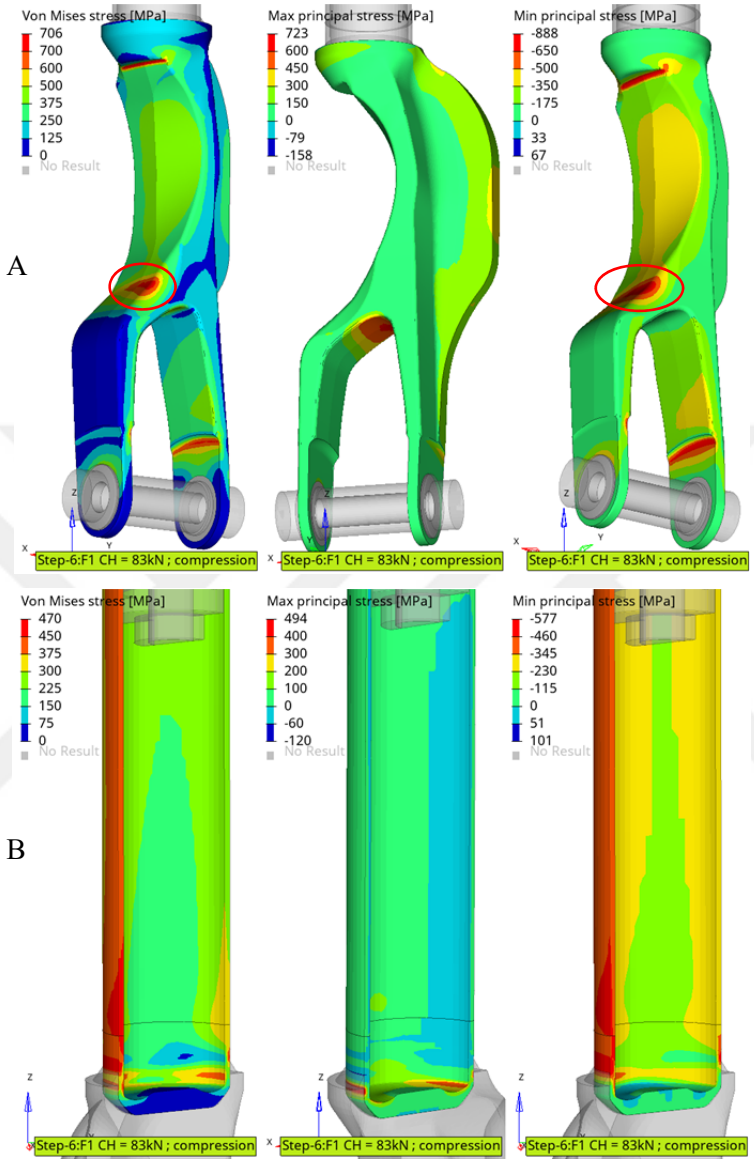


Figure 4.7. Analysis results for (A) yoke variant 1 with (B) E235+C tube. Misalignment with maximum Chinese load case that the shock absorber can handle (Tenneco CAE analysis report #3455).

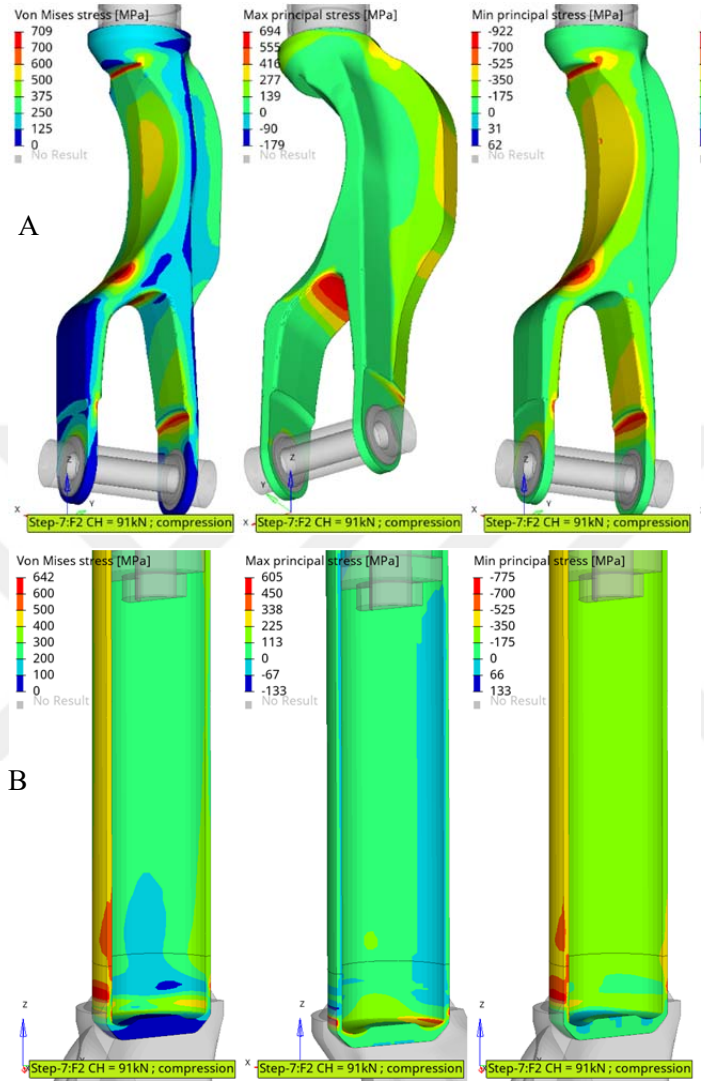


Figure 4.8. Analysis results for (A) yoke variant 1 with (B) E335+C tube. Misalignment with maximum CH load case 91kN (Tenneco CAE analysis report #3455).

When the yoke variant 1 (Figure 3.14.A) was equipped with pressure tube E335+C, it was able to comply with the requirements of minimum 0.2mm plastic deformation (Figure 4.8) however, due to buckling forces that were caused by the yoke variant 1, the material was redistributed without changing the weight of the

yoke and packaging requirement. Therefore, the stiffness of the yoke has been increased and assembly was done with E335+C as a precaution.

Even though the yoke variant 1 with pressure tube E335+C is able to provide plastic deformation of 0.019mm, the selection of the yoke was made for a stiffer one (Figure 4.9). This is due to the precaution taken against the undefined forces that might act on the shock absorber. Not all road loading data reflects the real time scenario and some cases are very difficult to recreate with the available testing equipment.

Besides the material strength, following factors might also affect the strength of the shock absorber:

- Clearance between the yoke and ball joint and bolt pre-tension load
- Magnitude and direction of side loads
- Length of the shock and spring load application point
- Geometry of welded connection between tube and yoke
- Bushings/joints characteristic

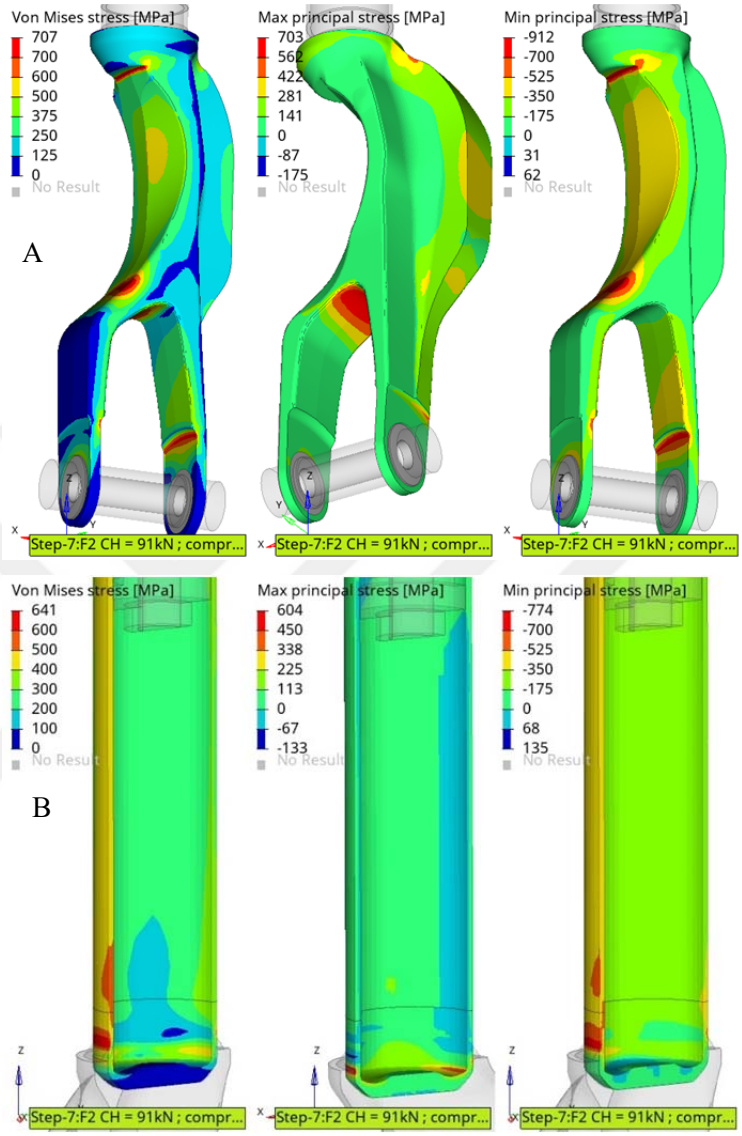


Figure 4.9. Analysis results for (A) Yoke variant 2 with (B) E335+C tube. Misalignment with maximum CH load case 91kN (Tenneco CAE analysis report #3455).

4.2. Augmented Reality Results

An Android device was used for the application. After exporting the scenes as shown in Figure 3.27, it is possible to find a file with .apk extension that contains the model guide lines. After installing the mobile application, it is ready to be used on the real object.

When the generated 2D guidelines (Figure 3.26) match with the object, AR app brings the object that was used as model target (Figure 4.10).

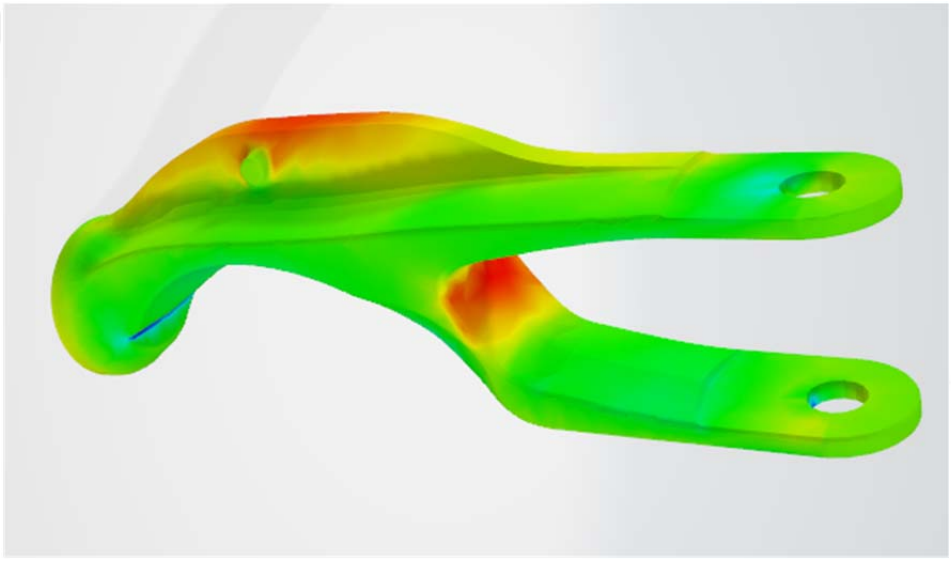


Figure 4.10. Exported 3D model of the yoke analysis results in the colors obtained after static analysis in Ansys.

After the guide view recognizes the object, it lays the 3D object onto the real part once it matches the views (Figure 4.11).

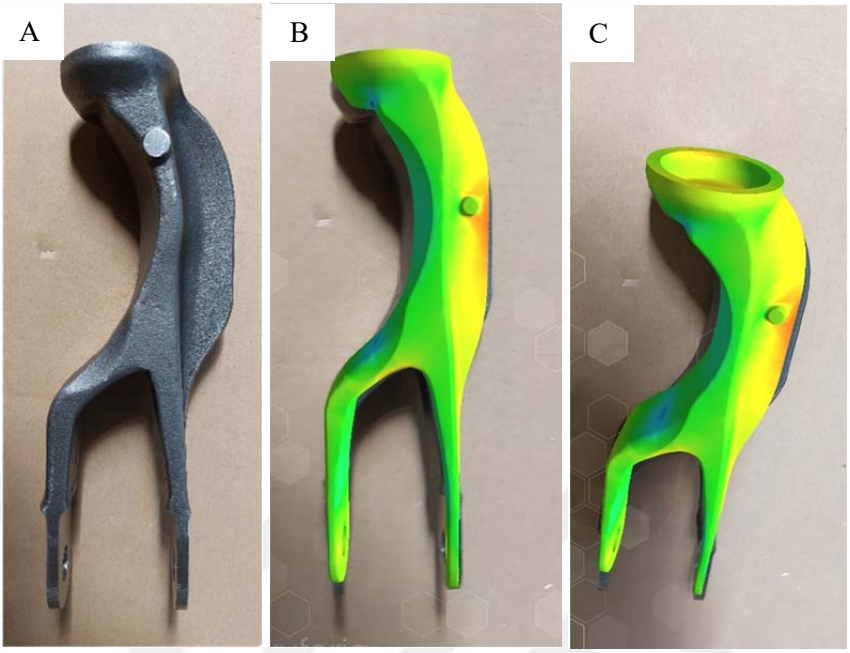


Figure 4.11. Mobile view of (A) original 3D view of object, (B) object matched with the guide view, (C) rotated view of the object.

5. CONCLUSION

The design of a shock absorber yoke for a vehicle that requires specific drive characteristics and therefore specific loading cases and representation of it in an AR platform have been represented in this study. In order to finalize a critical element of a shock absorber, topology optimization was used to iterate two different designs to obtain the most suitable solution, which was in the end decided to be the third iteration.

A shock absorber yoke is usually a complex design work given the packaging requirements of the vehicle. They can come in any shape and volume that complies the requirements. The design challenge is to avoid buckling of the pressure tube given the connection between the lateral load stiffness of the yoke and forces transferred to the pressure tube in the compressed length scenario. Changes have been introduced into the yoke design based on the analysis results and finally obtained a design that works well with the given loading cases. Additionally, preparing the technical drawing where the dimensional tolerances will play a crucial role was one of the most challenging parts in finalizing the design.

Together with the supplier of the yokes, the final shape is decided. Because the manufacturing method of this yoke contains casting and milling, it is wise to consult with suppliers and their production capabilities. Finalizing the design does not end with obtaining the completion of the analysis and modifying parts. The separation line of the cast, additional support material for the milling fixture etc. are decided and added to the part without compromising the structural integrity of the design.

This decision might be questioned when considering the matter in a financial perspective. Yoke is manufactured via casting method and after the casting, it is subjected to CNC machining in order to get the cavity and mounting legs according to tolerances set by engineers. But ordering two different types of

yokes will cost double considering that the forging equipment must be ordered twice for two different yokes.

After finalizing the yoke design, other components of the shock absorber have been brought together to create the complete assembly (Figure 5.1). After the design phase completed, parts and shock absorber prototypes have been built in order to carry out the internal and customer testing. Before moving into the serial production, several tests are needed to be completed on the customer vehicle. This is to decide all the modular components such as spring, top mount and compression bumpers. And most importantly, valving is decided after these tests. Testing engineers validate the valving systems by driving the vehicle while the prototype shock absorbers are installed.



Figure 5.1. Complete assembly of shock absorber.

The completion of the assembly and design validation with internal tests does not mean that the product is ready to be produced about hundreds of thousands of them. There are many other tests where a shock absorber must perform with real world conditions. When the designs are agreed by engineers and customer, design of special units are completed which engineers are able to disassemble the whole module and modify the core components such as valving system including piston. These special units are taken to the events which are called Ride Work where customers and ride engineers mount the units on the car and test the characteristics of the car. Even though initial analysis is made on which valving system to be chosen, it is often incorrect due to highly changeable mass and other properties of the vehicle. After the confirmation of the units with chosen

valving system, there will be testing units built which are Production Intended Design which means it is no longer modifiable by anyone and only way to reach the core components are via breaking the shock absorber which is not suggested due to safety reasons.

The work later has been visualized in an AR environment using Unity and Vuforia engine. Necessary analysis data of the yoke was exported in 3D shaded format and imported into Unity via Vuforia engine. Completing the steps, the analysis of the model was able to be viewed in a mobile device. The most challenging part was to export the 3D information with the shading that was obtained after the analysis. Exporting the obtained part usually loses this information but, in the end, the goal was achieved with exporting the results in .ply format, then using a software called MeshLab to convert the file into .obj format. Even though Microsoft's 3D viewer was able to display the shading, Unity was not able to recognize. Therefore, adding the file that contains color spectrum information to the .obj file has solved the problem.

For designers, visualizing the designs and analysis of them on real parts are always helpful. In case of having no access to CAD tools but having a mobile device to visualize the data always makes decision making easier. This work has been particularly helpful to decide what design changes to be introduced after the prototype building.

Moreover, the use of augmented reality can be extended for the modular unit analysis and flow analysis inside the shock absorber. Like the most of the components of a vehicle, shock absorber has a very complex design. It would be beneficial to build an AR application where engineers are able to visualize the flow within the pressure tube and using the quarter car 3D models, the simulation can be carried out to obtain a close-to-real analysis and visualization of them. This way, engineers would be able to decide on components which provide the characteristics to the vehicle.

REFERENCES

Abdul Halim, A. Z., 2018. Applications of Augmented Reality for Inspection and Maintenance Process in Automotive Industry. Journal of Fundamental and Applied Sciences, 10(3S): 412-421.

Arikere, A., Saravana Kumar, G. and Bandyopadhyay, S., 2010, December. Optimisation of double wishbone suspension system using multi-objective genetic algorithm. In Asia-Pacific Conference on Simulated Evolution and Learning (pp. 445-454).

Azuma, R. T., 1997. A Survey of Augmented Reality. Presence: Teleoperators & Virtual Environments, 6(4): 355-385.

Bai, Z. and Blackwell, A. F., 2012. Analytic Review of Usability Evaluation in ISMAR. Interacting with Computers, 24(6): 450-460.

Bendsoe, M. and Sigmund, O., 2003. Topology Optimization: Theory, Methods and Applications. Berlin.

Bendsøe, M. P. and Kikuchi, N., 1988. Generating Optimal Topologies in Structural Design Using a Homogenization Method. Computer Methods in Applied Mechanics and Engineering, 71(2): 197-224.

Bendsøe, M. P. and Kikuchi, N., 1988. Generating Optimal Topologies in Structural Design Using a Homogenization Method. Computer Methods in Applied Mechanics and Engineering, 71(2): 197-224.

Bendsøe, M. P., 1995. Optimization of Structural Topology, Shape, and Material. Heidelberg, Springer, p. 6-16.

Broxterman, S., 2017. Using Topology Optimization for Actuator Placement within Motion Systems.

Cavazzuti, M., Baldini, A., Bertocchi, E., Costi, D., Torricelli, E. and Moruzzi, P., 2010. High Performance Automotive Chassis Design: A Topology Optimization Based Approach. Journal of Structural and Multidisciplinary Optimization, 41(1): 45-56.

Cavazzuti, M., Splendi, L., D'Agostino, L., Torricelli, E., Costi, D., and Baldini, A., 2012. Structural Optimization of Automotive Chassis: Theory, Set Up, Design. In Problemes inverses, Controle et Optimisation de Formes 6.

Chang, J. W. and Lee, Y. S., 2008. Topology Optimization of Compressor Bracket. Journal of Mechanical Science and Technology, 22: 1668-1676.

Chiandussi, G., Gaviglio, I. and Ibba, A., 2004. Topology Optimisation of an Automotive Component without Final Volume Constraint Specification. Advances in Engineering Software, 35(10-11): 609-617.

Chuang, C. H., Chen, S., Yang, R. J. and Vogiatzis, P., 2018. Topology Optimization with Additive Manufacturing Consideration for Vehicle Load Path Development. International Journal for Numerical Methods in Engineering, 113(8): 1434-1445.

Dems, K., 1991. First-And Second-Order Shape Sensitivity Analysis of Structures. Structural Optimization, 3(2): 79-88.

Dey, A., Billinghurst, M., Lindeman, R. W. and Swan, J. E., 2018. A Systematic Review of 10 Years of Augmented Reality Usability Studies: 2005 to 2014. Frontiers in Robotics and AI, 5:37.

Dietsche, K. and Reif, K., 2022. Automotive Handbook, (K. Dietsche, ed.) Shock Absorbers and Vibration Absorbers. Karlsruhe, Robert Bosch GmbH, p. 1136-1256.

Dini, G. and Dalle Mura, M., 2015. Application of Augmented Reality techniques in through-life engineering service. In proceedings of the 4th International Conference on Through Life Engineering Services, p. 14-23.

Duysinx, P. and Bendsøe, M. P., 1998. Topology Optimization of Continuum Structures with local Stress Constraints. International Journal for Numerical Methods in Engineering, 43(8): 1453-1478.

Fonseca, D., Martí, N., Redondo, E., Navarro, I. and Sánchez, A., 2014. Relationship between Student Profile, Tool Use, Participation. and Academic Performance with the Use Of Augmented Reality Technology for Visualized Architecture Models. Computers in Human Behavior, 31: 434-445.

Ghasemalizadeh, O., Taheri, S., Singh, A. and Goryca, J., 2014. Semi-active Suspension Control Using Modern Methodology: Comprehensive Comparison Study. *arXiv preprint arXiv:1411.3305*.

Haugstvedt, A. C. and Krogstie, J., 2012. Mobile Augmented Reality for Cultural Heritage: A Technology Acceptance Study, in ISMAR 2012-11th IEEE International Symposium on Mixed and Augmented Reality 2012, Science and Technology Papers (Atlanta, GA), p. 247–255.

Henderson, S. J. and Feiner, S., 2009. Evaluating the Benefits of Augmented Reality for Task Localization in Maintenance of an Armoured Personnel Carrier Turret. in Science and Technology Proceedings - IEEE 2009 International Symposium on Mixed and Augmented Reality, ISMAR 2009 (Orlando, FL), p. 135–144.

Huang, J. M., Ong, S. K. and Nee, A. Y., 2017. Visualization and Interaction of Finite Element Analysis in Augmented Reality. Computer-Aided Design, 84: 1-14.

Ibáñez, M. B., Di Serio, Á., Villarán, D. and Kloos, C. D., 2014. Experimenting with Electromagnetism Using Augmented Reality: Impact on Flow Student Experience and Educational Effectiveness. Computers & Education, 71: 1-13.

Irizarry, J., Gheisari, M., Williams, G. and Walker, B. N., 2013. InfoSPOT: A Mobile Augmented Reality Method for Accessing Building Information through a Situation Awareness Approach. Automation in Construction, 33: 11-23.

Jankovics, D. and Barari, A., 2019. Customization of Automotive Structural Components Using Additive Manufacturing and Topology Optimization. IFAC-PapersOnLine, 52(10): 212-217.

Kilian, S., Zander, U. and Talke, F. E. 2003. Suspension modeling and Optimization Using Finite Element Analysis. Tribology International, 36(4-6): 317-324.

Kingman, J., Tsavdaridis, K. D. and Toropov, V. V., 2015. Applications of Topology Optimization in Structural Engineering: High-Rise Buildings and Steel Components. Jordan Journal of Civil Engineering, Leeds,159(3097): 1-23.

Li, W. K., Nee, A. Y. C. and Ong, S. K., 2018. Mobile augmented reality visualization and Collaboration Techniques for On-Site Finite Element Structural Analysis. International Journal of Modeling, Simulation, and Scientific Computing, 9(3): 1840001.

Li, W., Nee, A. Y. and Ong, S. K., 2017. A State-of-the-Art Review of Augmented Reality in Engineering Analysis and Simulation. Multimodal Technologies and Interaction, 1(3): 17.

Michell, A. G. M., 1904. LVIII. The Limits of Economy of Material in Frame-Structures. The London, Edinburgh, and Dublin Philosophical Magazine and Journal of Science, 8(47): 589-597.

Morgan, H.D., Levatti, H.U., Sienz, J., Gil, A.J. and Bould, D.C., 2014. GE Jet Engine Bracket Challenge: a Case Study in Sustainable Design. Sustainable Design and Manufacturing, 14(2), p. 95-107.

Murr, L. E., Gaytan, S. M., Ramirez, D. A., Martinez, E., Hernandez, J., Amato, K. N., Patrick W. S., Francisco, R. M. and Wicker, R. B., 2012. Metal Fabrication by Additive Manufacturing Using Laser and Electron Beam Melting Technologies. Journal of Materials Science & Technology, 28(1): 1-14.

Ng-Thow-Hing, V., Bark, K., Beckwith, L., Tran, C., Bhandari, R., and Sridhar, S., 2013, User-Cantered Perspectives for Automotive Augmented Reality, IEEE International Symposium on Mixed and Augmented Reality-Arts, Media, and Humanities, ISMAR-AMH, p. 13–22.

Ning, Y. W., Suprobo, P., Jeong, G. D. and Ting, E. C., 1993. A Regional Mixed Refinement Procedure for Finite Element Mesh Design. Finite Elements in Analysis and Design, 13(4): 299-318.

Nowaczyk, M. and Paesmans, J., 2010, Triple Tube Shock Absorber Having a Shortened Intermediate Tube, U.S. Patent No. 2010/019308 A1, U.S. Patent and Trademark Office. https://rb.gy/ynctcv

Pedersen, C. B., 2003. Topology Optimization Design of Crushed 2D-Frames for desired Energy Absorption History. Structural and Multidisciplinary Optimization, 25(5): 368-382.

Pedersen, C. B., 2004. Crashworthiness Design of Transient Frame Structures Using Topology Optimization. Computer Methods in Applied Mechanics and Engineering, 193(6-8): 653-678.

Querin, O. M., Victoria, M., Gordoa, C. A., Ansola, R. and Martí, P., 2017. Topology Design Methods for Structural Optimization. London, Academic Press, p. 35-45.

Rivara, M. C., 1991. Local Modification of Meshes for Adaptive and/or Multigrid Finite-Element Methods. Journal of Computational and Applied Mathematics, 36(1): 79-89.

Rozvany, G. I., Zhou, M. and Birker, T., 1992. Generalized Shape Optimization without Homogenization. Structural Optimization, 4(3): 250-252.

Schneiders, R. and Debye, J., 1995. Refinement Algorithms for Unstructured Quadrilateral or Brick Element Meshes. Modeling, Mesh Generation and Adaptive Numerical Methods for Partial Differential Equations.

Sigmund, O. and Maute, K., 2013. Topology Optimization Approaches. Structural and Multidisciplinary Optimization, 48(6): 1031-1055.

Sun, S., Brandt, M. and Easton, M., 2017. Powder Bed Fusion Processes. In (M. Brandt, ed.) Laser Additive Manufacturing. Sawston, Woodhead Publishing, p. 55–77.

Suzuki, K. and Kikuchi, N., 1991. A Homogenization Method for Shape and Topology Optimization. Computer Methods in Applied Mechanics and Engineering, 93(3): 291-318.

Wang, L., Basu, P. K. and Leiva, J. P., 2004. Automobile Body Reinforcement by Finite Element Optimization. Finite Elements in Analysis and Design, 40(8): 879-893.

Yang, R. J., Chuang, C-H., Che, X. and Soto, C., 2000. New Applications of Topology Optimization in Automotive Industry. International Journal of Vehicle Design, 23(1-2): 1-15.

Yang, R. J., Rui, Y., Mohammed, A. and Singh, G., 1996. Spot Weld/Adhesive Pattern Optimization. In International Design Engineering Technical Conferences and Computers and Information in Engineering Conference (Vol. 97591, p. V003T03A002). American Society of Mechanical Engineers.

CURRICULUM VITAE

Halit Doğrusoz finished high school in 2012 and started bachelor's degree of Mechanical Engineering at Erciyes University in Kayseri. He studied English preparation school between 2012-2013 started mechanical engineering in 2014. During his studies, he has attended one semester of Erasmus program in West Pomeranian University of Technology. After his graduation, he started his master's degree classes at Çukurova University. Meanwhile, he has been accepted for the internship at EMT-Systems in Gliwice, Poland and after the internship period, he was employed in the company. In 2021 March, he has been employed by Tenneco Automotive Inc. as a mechanical designer.

APPENDIX

A.1. 38MnVS6 and EN 10083-2 Material Specifications

General Information

Grade 38MnVS6 is a micro-alloyed medium carbon steel for general purposes. The steel is recommended for applications demanding high mechanical properties and smooth surfaces.

482A - Ingot cast variant

7221 - Continuous cast variant.

SB9857 - Continuous cast variant.

For additional Heat Treatment Data, please visit the Heat Treatment Guide

Similar designations

39MnV5, 1.1303

Chemical composition

Variant	Cast	Di	Weldability		C %	Si %	Mn %	P %	S %	Cr %	Ni %	Mo %	V %	Cu %	Al %	N %
482A	IC	3.5	CEV 0.75_{max}	Min	0.37	0.35	1.25	-	0.020	0.20	0.15	-	0.110	-	-	-
			Pcm 0.53_{max}	Max	0.40	0.42	1.35	0.025	0.028	0.26	0.20	0.05	0.150	-	-	-
7221	CC	2.81	CEV 0.68_{max}	Min	0.36	0.30	1.00	-	0.010	-	-	0.02	0.100	-	0.010	0.0100
			Pcm 0.498_{max}	Max	0.41	0.50	1.40	0.025	0.025	0.30	-	0.06	0.200	-	0.040	0.0180
SB9857	CC		CEV 0.7_{max}	Min	0.37	0.30	1.20	-	-	-	-	-	0.110	-	-	-
			Pcm 0.51_{max}	Max	0.43	0.50	1.40	0.025	0.030	0.30	-	-	0.160	-	-	-
38MnVS6 EN 10267:1998	Std		CEV 0.72_{max}	Min	0.34	0.15	1.20	-	0.020	-	-	-	0.080	-	-	-
			Pcm 0.5_{max}	Max	0.41	0.80	1.60	0.025	0.060	0.30	-	-	0.200	-	-	-

Mechanical Properties

Variant	Condition	Format	Dimension [mm]	Yield strength min [MPa]	Tensile strength [MPa]	Elongation A_5 [%]	Reduction of area Z_{min} [%]	Hardness	Impact (ISO-V) $strength_{min}$
482A	+AR	Round bar	90 < 140	580*	850-1000	14	-	< 300 HB	20 °C 20 J (long)
7221	+AR	Round bar	22 < 120	580	850-1000	12	25	250-300 HB	-
SB9857	+AR	Round bar	20 < 95	580**	850-1000	14	-	250-300 HB	0 °C 0 J (long)
38MnVS6 EN 10267:1998	+AR	All formats	-	520**	800-950	12	25	-	-

$Rp_{0.2}$ * R_{eh}, ** R_{el}

Transformation temperatures

	Temperature °C
MS	330
AC1	720
AC3	780

C45 EN 10083-2

Standards

EN 10083-2

Chemical composition

C	0.42 - 0.50	**Si**	< 0.4	**Mn**	0.5 - 0.8	**P**	< 0.045
S	< 0.045	**Cr**	< 0.4	**Mo**	< 0.1	**Ni**	< 0.4
Fe	Rest						

Properties

By EN 10083-2

+N

Thickness: < 16 mm ;

Yield Strength: > 340 MPa
Tensile Strength: > 620 MPa
Elongation: > 14 %

Thickness: 16 - 100 mm ;

Yield Strength: > 305 MPa
Tensile Strength: > 580 MPa
Elongation: > 16 %

Thickness: > 100 mm ;

Yield Strength: > 275 MPa
Tensile Strength: > 560 MPa
Elongation: > 16 %

+QT

Diameter: < 16 mm ;

Yield Strength: > 490 MPa
Tensile Strength: 700 - 850 MPa
Elongation: > 14 %
Reduction of area: > 35 %

Diameter: 16 - 40 mm ;

Yield Strength: > 430 MPa
Tensile Strength: 650 - 800 MPa
Elongation: > 16 %

A.2. E235+C and E335+C Material Specifications

Global Monotube Material Specification

1.0 Scope

This specification covers SAE 1008/1015 hot rolled, E235 +C, S235JR (ST37-2) cold or hot rolled, electric welded, normalized and redrawn steel tubing suitable for fabricating monotube tubing.

2.0 Reference
2.1 Index

Scope	1.0
Reference	2.0
Engineering Background	3.0
Requirements	4.0
Testing & Certification	5.0
Packaging & Shipping	6.0

2.2 Applicable Documents at the latest Revision Levels:

ASTM A1008/A1011, ASTM A366, ASTM A513, ASTM E8, ASTM A29, ASTM A370, ASTM A568/568M, ASTM E18, ASTM A700, ASTM E309, ASTM E425, ASTM A450, ASTM A1008/A1011, EN10305-2, Q/BQB 303, EN ISO 6892-1, EN ISO 10893.

3.0 Engineering Background

3.1 Parts Processing Chronology

The parts shall be cut to length, double end chamfered, washed and hot formed base end. The final assembly is crimped and spun over.

4.0 Requirements
4.1 General Requirements
Except as otherwise noted in this specification or the purchase order, this material shall conform to the latest revision level of ASTM A366 or equivalent in Europe and China. The material will be supplied in tube form. The inside diameter is to be finished especially smooth and must be free from pits, scores, scratches or other defects. The tubes shall be free from kinks and other damage. The cut surfaces have to be round, parallel to each other and burr free. The material shall be free from hard spots, segregation, laminations, excessive flutes or stretcher strains. The vendor shall have all tube checked visually and tested on air tightness by ultrasonic or with eddy current in accordance with ASTM E309-latest revision level or equivalent in Europe and China. (ASTM E309 is Eddy Current Specific).

Any process, supplier or material changes made to this product requires prior approval by Tenneco Engineering Department or must be in accordance with Tenneco deviation policy reference document.

4.2 Chemical limits

Element	Chemical composition [%]		
	North America SAE 1008/1015	Europe E235 +C	China S235JR (ST37-2)
Carbon	0.02 - 0.18	0.02 - 0.17	0.02 - 0.17
Manganese	0.20 - 0.85	0.20 - 1.20	1.40 maximum
Phosphorous	0.05 maximum	0.025 maximum	0.035 maximum
Sulfur	0.05 maximum	0.025 maximum	0.035 maximum
Silicon	-	0.35 maximum	0.35 maximum
Aluminum	-	0.02 - 0.07	-

4.3 Physical Requirements

4.3.1 Ovality: 0.040mm (.0016") T.I.R.(Total Indicator Reading)(30mm)
I.D. to be minimum diameter 30.150mm (1.1870") and maximum to be 30.181mm (1.1882") at any place.
O.D. to be 33.030mm +/- 0.05mm (1.3003") for (30mm).
Wall thickness (30mm) to be 1.400mm (0.0551") ref.
Minimum burst pressure 540Bar (7832.052Psi).

Ovality: 0.040mm (.0016") T.I.R. (Total Indicator Reading)(36mm)
I.D. to be minimum diameter 36.000mm (1.4173") and maximum to be 36.040mm (1.4189") at any place.
O.D. to be 40.000mm +/- 0.05mm (1.5748") for (36mm).
Wall thickness (36mm) to be 2.000mm (0.0787") ref.
Minimum burst pressure 630Bar (9137.394Psi).

Ovality: 0.040mm (.0016") T.I.R. (Total Indicator Reading)(36mm)
I.D. to be minimum diameter 36.000mm (1.4173") and maximum to be 36.040mm (1.4189") at any place.
O.D. to be 38.800mm +/- 0.05mm (1.5276") for (36mm).
Wall thickness (36mm) to be 1.40mm (0.0551") ref.
Minimum burst pressure 440Bar (6831.672Psi).

Ovality: 0.040mm (.0016") T.I.R. (Total Indicator Reading)(46mm)
I.D. to be minimum diameter 46.000mm (1.8110") and maximum to be 46.040mm (1.8125") at any place.
O.D. to be 50.000mm +/- 0.05mm (1.9685") for (46mm).
Wall thickness (46mm) to be 2.000mm (0.0787") ref.
Minimum burst pressure 490Bar (7106.862Psi).

4.3.2 Straightness: 0.180mm (.0071") per 254mm (10") maximum.

4.3.3 Surface Finish Requirements:

4.3.3.1 A minimum of two readings are to be taken in the longitudinal direction. The readings are to be a minimum of 90 degrees apart on the inside diameter of the tubes.
Profilometer setup - Cutoff: 0.8 mm & Measurement length: 4.0 mm

4.3.3.2 Surface Finish Acceptance Criteria

Ra: 0.40 micrometer (maximum)
Rz: 4.00 micrometer (maximum)

Note: Unless otherwise stated for physical requirements the purchase order will be the prevailing document.

4.4 Mechanical Requirements (Per Production Lot)

Tensile testing to be performed in accordance with the latest revision level of ASTM E8 with the following conditions:

1. Samples must be excised from full finished tubes parallel to the drawing direction in conformance with Figure 12 of ASTM E8 for North America or EN ISO 6892-1 for Europe.

2. Sample dimensions must conform to those specified in Figure 13, specimen 1, per ASTM E8 for North America or Figure 14 per EN ISO 6892-1 for Europe.

3. Ends of tensile specimen can be flattened to accommodate gripping of sample long as flattening does not extend into the reduced section of the specimen.

4. Gage marks can be lightly punched or scribed on layout dye. Marker is not acceptable.

5. The test speed shall be as follows:
Free running cross head speed of 1/16 inch per minute, per 1 inch of gage length through yield.

Free running cross head speed of 1/2 inch per minute, per 1 inch of gage length through tensile.

Mechanical properties of tested specimen must meet the following strength level.

Yield Strength	68,000 - 79,800 psi (470 - 550 MPa)
Tensile Strength	70,000 - 82,600 psi (490 - 570 MPa)
Elongation	10% minimum
Hardness (Ref)	HRb 80-87

In the event that a discrepancy in tensile test results arises, samples will be sent to an independent certified lab of Tenneco's choice for referee testing.

4.5 Flare Test: Tube must be expanded with a tapered plug from 30 degrees -2 degrees to a diameter of 39.60mm (1.60") for 36mm, 50.60mm (2.00") for 46mm and 33.20mm (1.30") for 30mm without any rupture of the seam weld.(10% over maximum diameter).

5.0 Testing and Certification

5.1 Certification from the vendor (Supplier) is required for each production lot(A production lot is defined as material which meets all the following criteria),
1) Same heat of steel/chemical composition,
2) Sample pipe hollow size and
3) Consecutive thermal and mechanical processing.

The certification shall include chemical composition, T.I.R.(Total Indicator Reading) and mechanical properties. This will be used to verify the material meets all the requirements of this specification.

6.0 Packaging and Shipping

According to plant policy.